Advancing Nanoelectronics Applications: Progress in Non van der Waals 2D Materials

*Hongze Gao[1], Zifan Wang[1], Jun Cao[1], Yuxuan Cosmi Lin[2], and Xi Ling** [1,3]

[1]Department of Chemistry, Boston University

590 Commonwealth Ave., Boston, MA, 02215, U.S.

[2]Department of Materials Science and Engineering, Texas A&M University

575 Ross St., College Station, TX, 77843, U.S.

[3]Division of Materials Science and Engineering, Boston University

15 St Mary's St., Boston, MA, 02215, U.S.

Email: xiling@bu.edu

Abstract

Extending the inventory of two-dimensional (2D) materials remains highly desirable given their excellent properties and wide applications. Current studies on 2D materials mainly focus on the van der Waals (vdW) materials since the discovery of graphene, where properties of atomically thin layers have been found distinct from their bulk counterparts. Beyond vdW materials, there are abundant non vdW materials that can also be thinned down to 2D forms, which are still in its early stage of exploration. In this review, we focus on the downscaling of non vdW materials into 2D forms to enrich the 2D materials family. This under-explored group of 2D materials could show potential promise in many areas such as electronics, optics, and magnetics, as that has happened in the vdW 2D materials. Hereby, we will focus our discussion on the electronic properties and applications of them. We aim to motivate and inspire fellow researchers in the 2D materials

community to contribute to the development of 2D materials beyond the widely studied vdW layered materials for electronic device applications. We also give our insights on the challenges and opportunities to guide researchers who are desirous of working in this promising research area.

Keywords

2D materials, non vdW materials, 2D electronic devices, 2D heterostructures, 2D materials synthesis, 2D transistors, band structure modifications, 2D dielectrics

Vocabulary

vdW materials	A group of materials that are composed of atomic layers, where van der Waals interactions instead of chemical bonds hold adjacent layers together.
Non vdW materials	A group of materials where chemical bonds are the only kind of interactions between atoms. No van der Waals interactions are involved.
2D materials	Materials containing single or a few layers of atoms along one dimension, with thickness ranging from sub-1-nm to tens of nm. The materials exhibit much bigger size along the other two dimensions.
2D electronics	Electronic devices based on 2D materials.
Heterostructures	The structures composed of multiple different materials. Each material plays a specific role in this structure.

The discovery of graphene in 2004 sparked a dramatic increase in two-dimensional (2D) materials research and the repertoire of reported 2D materials family has since expanded.[1–4] 2D crystals composed of single or few layers of atoms often display extraordinary chemical, optical, and electronic properties compared with their bulk 3D counterparts due to quantum confinement at the 2D limit.[5–11] In the past two decades, 2D materials have been a wonderful playground for many interesting chemistry, physics, engineering and quantum science.[12–19] Beyond the fundamental studies, 2D materials have also shown great potential in diverse fields of applications including nanoelectronics,[20–24] quantum information,[16,17,25,26] and flexible electronics.[27,28] There are many excellent review articles summarizing the recent progress in this field.[29–34] The fascinating promise of 2D materials has stimulated the exploration of both more materials and complex quantum structures.[2,4,30,35] The majority study in the 2D materials field have been focusing on van der Waals (vdW) 2D materials such as graphene, transition metal dichalcogenides (TMDs) and hexagonal boron nitride (hBN). The exploration of non vdW 2D materials, however, is still in its early stage mostly due to the technical challenges in their synthesis. As shown in Figure 1a, vdW crystals possess anisotropic internal interactions, where strong chemical bonds are formed in the basal plane of each atomic layer, and a weak vdW interaction holds different layers together. In contrast, vdW gaps are absent in non vdW crystals, and strong chemical bonds that require a high energy to break are present in all three dimensions. The difference in the anisotropy of interactions between vdW and non vdW crystals imposes a crucial discrepancy in scaling down these crystals into their 2D forms, *i.e.*, vdW 2D materials and non vdW 2D materials.

Owing to the strong chemical bonds in all directions, the widely adapted mechanical exfoliation approach (scotch tape method) is not useful to separate ultrathin layers from a bulk non vdW crystals. Meanwhile, although conventional thin film deposition techniques (*e.g.*, chemical

vapor deposition (CVD) and molecular beam epitaxy (MBE)) produce thin films with high quality and purity, they are not ideal to prepare high-quality samples when the film thickness comes to the sub-10-nm regime. Three models are commonly used to describe the growth mechanisms in conventional CVD and MBE: Frank–van der Merwe (layer by layer growth), Stranski–Krastanow (layer-island growth), and Volmer–Weber (island growth) model.[36] While different model is applied to describe a specific film depending on the lattice mismatch and the consequential strain between the substrates and deposited materials, most experimentally obtained films in the sub-10-nm regime exhibit island-like growth.[37–40] As a result, the deposited films usually possess rough surfaces (root-mean-square roughness over 1 nm) and small domain sizes.[38,40] The island-like growth inevitably leads to morphology and property modifications of ultrathin films from their bulk counterparts, which in most cases deteriorates the performance. For example, drastic charge scattering is observed in thermally deposited Cu and Si films below 10 nm,[41,42] and GaN prepared by MBE tends to form quantum dots instead of layers in the few nanometers regime.[39,43] Therefore, thin films prepared by conventional deposition techniques will not be the focus of discussion in this article. Instead, we will focus on the ultrathin layers of non vdW crystals with smooth surfaces, fabrication-friendly sample size (> 10 μm), and thickness of few to tens of nanometers. Alternative synthesis methods are in great demand to produce and study non vdW materials in 2D form and will be discussed in a later session of this article.

While the synthesis of non vdW 2D materials presents considerable technical challenges, there is a growing imperative to investigate these materials to introduce more functionalities and to enhance the performance of electronic devices based on 2D materials. Notably, significant research efforts have been directed towards exploring vdW 2D materials, leveraging their high charge carrier mobility (as observed in graphene) and appropriate bandgap energy (as seen in

TMDs).[18,44,45] The exceptional properties of vdW 2D materials position them as promising candidates for the next generation of electronic devices, and supplements for the existing Complementary Metal-Oxide-Semiconductor (CMOS) technologies.[34,46,47] However, a few key characteristics are missing in vdW 2D materials, leaving a gap towards their industrial applications. For instance, TMDs exhibit a pronounced Fermi level pinning (FLP) effect, resulting in suboptimal charge carrier mobilities and high contact resistances.[22,23,48–52] Furthermore, the scarcity of wide bandgap semiconductors and insulators within vdW 2D materials poses another challenge. According to Cheon *et al.*, the majority (>85%) of vdW 2D materials have bandgap energies below 2.5 eV,[53] whereas a wider bandgap is crucial for dielectric materials and power electronics.[54] Although these essential properties are not common among vdW 2D materials, they have been observed in various bulk non vdW crystals. For instance, germanium (Ge) exhibits high electron and hole mobility, and many metal oxides display wide bandgaps and high breakdown fields.[55,56] Exploring the downscaling of these non vdW crystals could introduce valuable supplements to the inventory of 2D materials.

Moreover, non vdW materials are more abundant in nature, offering more possibilities and expanding the design space of 2D materials. In Figure 1b, we summarize the elements present in the experimentally achieved vdW and non vdW materials, in both 2D and bulk form, in a periodic table.[20,29,58,60,62-82] A list of 2D material examples for each element is summarized in Table 1. Calculations predicted that only less than 2.5% of all experimentally known crystals (2,662 out of 108,423) possess weak vdW interactions, which could potentially allow down-scaling of the crystal into their low-dimensional form using conventional exfoliation method.[81] Nevertheless, experimentally achieved vdW 2D materials are far less than the aforementioned calculation.[67,74–76,82] In table 1, 55 out of 111 elements (inert gas elements excluded) have been involved in vdW

2D materials, 53 elements in non vdW 2D materials, while 47 elements have not been reported in any 2D materials yet. Therefore, there is plenty of room to explore the downscaling of non vdW crystals into their 2D forms, including synthesis, properties, and application investigations. Despite in the early stage, over a dozen of non vdW 2D materials with exciting properties are already synthesized and studied. We summarize them along with their studied properties (*e.g.*, bandgap, sizes, and key properties) for electronics applications in Table 2 for inspirations.[56-59,72,75–89] These examples show great promises of non vdW 2D materials in enriching the 2D family with desired properties.

In this work, we show how non vdW 2D materials can fill the gaps of current vdW 2D materials study and extend the blueprint of future 2D electronics. We will elaborate on the following aspects: (1) the challenges and recent progresses in the synthesis of non vdW 2D materials; (2) the properties modification of non vdW crystals at the low dimension; (3) exploration of the role of non vdW 2D materials in electronic devices; (4) the fabrication of clean and sharp interface in heterostructures enabled by atomic substitution approach and performance improvement. Reflected from these aspects, we will present our insights on future directions to inspire researchers who are interested in contributing to this emerging field.

Challenges and recent progresses in the synthesis of non vdW 2D materials

For the widely studied vdW 2D materials such as MoS_2, there is a vdW gap between two adjacent layers. The weak vdW interactions enables the separation of monolayers and few layers from their bulk crystals through the top-down mechanical exfoliation or grow into 2D films through the bottom-up CVD process.[45,98] Tremendous effort has been spent in recent years on making the 2D version of the vdW layered materials.[99–104] However, these methods are usually not adaptable to non vdW crystals. Common top-down synthesis approaches for vdW 2D materials such as the

scotch tape method hardly work for non vdW 2D materials owing to the strong bonding along all directions in non vdW crystals. The accessibility of bottom-up methods (*e.g.*, CVD) is also limited since dangling bonds are present along all crystal orientations and hence the flakes tend to grow in all the three dimensions. Thus, the study of non vdW 2D materials is significantly restrained by the technological difficulty in experimentally obtaining them. Increasing efforts have been made in very recent years to achieve the synthesis of non vdW 2D materials.[10,11,105,106] In this section, we summarize the five recently established approaches to obtain the 2D form of non vdW crystals and discuss their advantages and limitations.

Sonication-assisted exfoliation

Liquid phase exfoliation has been a widely applied approach to produce monolayer or few-layer nanosheets of vdW materials (*e.g.*, graphene, TMDs) with high purity and scalability.[103,107] Owing to the anisotropic bonding in vdW crystals, it requires different energies to break the interlayer and intralayer interactions. Hence, the energy carried by sonication wave can selectively break the interlayer interactions and separate nanosheets from the bulk crystal. The nanosheets are then stably dispersed in the liquid environment. In contrast to vdW materials, separating nanosheets of non vdW materials from their bulk counterparts is more challenging due to the chemical bonds extending in all three dimensions. Nevertheless, a topotactic deintercalation approach has been developed to break the anisotropic chemical bonds in a bulk non vdW crystal to obtain 2D sheets. This approach is commonly adapted to synthesize two groups of materials: (1) transition metal carbides, nitrides, and carbonitrides (MXenes), where a typical example is 2D $Ti_3C_2T_x$ (T_x stands for -O, -OH, or -F termination groups on the surface) produced by selectively etching the bulk phase precursors (Ti_3AlC_2);[108] (2) separation of group IV graphane analogues, *i.e.*, SiH, GeH, and SnH, from corresponding Zintl phases ($CaSi_2$, $CaGe_2$, and $BaSn_2$).[109] Aggressive chemicals such

as HF and HCl are introduced to selectively etch certain atomic layers in the bulk precursors, and hence to replace strong chemical bonding with weak vdW interactions. The etched sheets are then separated and dispersed in solvent. This approach has been applied to obtain different MXenes and graphane analogues, and has been discussed in many review papers in the 2D community.[6,109–113]

Although vdW gaps are absent in non vdW crystals, the energy required to break the chemical bonds varies along different crystal axes.[10,114] Hereby, it is reported that ultrasonic wave can selectively break the weaker chemical bonds along a certain crystal axis of some bulk non vdW crystals,[115–117] producing 2D films exfoliated and dispersed in the solvent. For example, Puthirath Balan *et al.* successfully isolated monolayer α-Fe_2O_3 (known as hematene) from non vdW iron ore hematite through sonication (Figure 2a).[114] The exfoliated monolayers have two dominating orientations [001] and [010]; these are the directions with weaker chemical bonds. 2D forms of other metal oxides (*e.g.*, ilmenene, magnetene and chromiteen) were also successfully exfoliated using this method.[11] Moreover, Liu *et al.* successfully obtained a variety of non vdW nanosheets (*e.g.*, FeOOH, PbS, $CaCO_3$) from their bulk crystals using similar sonication exfoliation,[118] and discovered that the orientations of these nanosheets are correlated to the cleavage planes of the pristine materials. Beyond the exciting progress in experiments, recent calculations have also predicted dozens of non vdW crystals with low exfoliation energies that can potentially be made into 2D form by sonication.[119,120] The sonication exfoliation method down-scales a variety of materials into their 2D form, which shows great potential in electrochemistry applications. However, the exfoliated flakes usually possess small lateral sizes (< 5 μm) and variable thickness with a wide range of distribution, which limits its application in 2D electronics.[10]

Chemical vapor deposition

CVD is one of the most widely employed bottom-up method to synthesize ultrathin 2D materials (both vdW and non vdW) with high quality and scalability.[77,80,121] During the CVD process (Figure 2b), vaporized precursors are first transported close to the growth substrate followed by a chemical reaction either in the gaseous phase or between the gaseous and solid precursors. Nucleation starts when the partial pressure of the gaseous compound reaches the supersaturation point.[98,122,123] After the nucleation process, the crystal starts to grow along a certain crystal orientation with lowest formation energy. Numerous vdW materials, such as graphene and TMDs, have been successfully synthesized through CVD.[123] Monolayer or few-layer form of non vdW materials, however, are much more challenging to realize using the conventional CVD method due to the absence of a saturated surface.

In the past few years, a few works have reported the synthesis of non vdW 2D materials through surface confined CVD processes. Two typical strategies have been applied to achieve the surface confined growth, *i.e.*, liquid metal synthesis,[77,80,90] and halide-induced self-limit growth.[94] Chen *et al.* demonstrated the growth of 2D GaN on liquid Ga spreading on W foil (Figure 2b) with thickness down to 4.1 nm.[90] During the CVD process, W atoms diffuse through the liquid Ga droplet to form W-Ga alloy, leaving an ultrathin (< 2 nm) pure Ga layer on the surface of the droplet. Upon the introduction of NH_3, the surface Ga layer reacts with NH_3 to form GaN, while the underneath W-Ga alloy exhibits negligible reactivity. Hence the nitridation reaction is confined on the surface of the Ga droplet to obtain 2D GaN. In another case, ultrathin non-layered Ge flakes were synthesized by Hu *et al.* using a halide-induced self-limited CVD growth.[94] KCl is introduced into the synthesis environment to facilitate the in-plane growth of Ge flakes. Calculations reveal that Cl atoms preferentially adsorb onto the (111) plane of Ge crystals and lowers the formation energy of Ge crystal, which promotes the growth rate along this crystal orientation beyond other

directions. 2D Ge flakes down to 8.5 nm thick have been achieved. These examples show that CVD method could be a powerful technique for non vdW 2D materials to achieve flakes with high crystallinity and clean surface, although the lateral size and thickness varies for different flakes even in one synthesis trial. Also, the growth process usually introduces other elements as impurities or dopants, such as W in single crystal GaN, which potentially modifies the properties of the synthesized flakes.[90,94] Moreover, the thinnest non vdW 2D materials prepared using CVD method are usually reported in the few-nanometer regime. Such thickness is equivalent to ~10 unit cell size. Synthesis of few- and the ultimate single-unit-cell-thick flakes remain challenging using CVD techniques at the moment.

Confinement heteroepitaxy growth

Epitaxial growth, a widely used technique for thin film deposition and hybrid nanostructure synthesis, involves the condensation of gaseous precursors on a substrate to form crystals.[124,125] Unlike standard CVD processes, epitaxial growth requires substrates with similar lattice parameters as the single crystal to be deposited. While extensively studied for preparing conventional semiconductor materials such as III-V compounds and quantum well superlattices, epitaxial growth also plays a crucial role in synthesizing vdW 2D materials.[43,126] For instance, wafer-scale monolayer MoS_2 films have been successfully synthesized on Al_2O_3 substrates, facilitating the application of MoS_2 in scalable nanoelectronic devices.[102] However, achieving ultrathin non vdW 2D materials through conventional epitaxial techniques remains challenging. The common thicknesses of the films significantly exceed the threshold for inducing the quantum confinement effect, which is also the critical range for observing the most intriguing phenomena.

In recent years, a modified epitaxial growth, *i.e.*, confinement heteroepitaxy growth (CHet), has been demonstrated as a feasible approach for the synthesis of ultrathin non vdW 2D materials.

Balushi *et al.* and Briggs *et al.* reported the synthesis of 2D GaN and 2D metals (Ga, In, Sn), respectively.[127,128] In both cases, an epitaxial graphene (EG)/SiC substrate is used for the growth, as demonstrated in the schematic drawing in Figure 2c. A gentle H_2 plasma is applied before supplying growth sources to generate defects in the EG film so that the precursors can diffuse through the defective EG film to reach the EG/SiC interface. The high energy EG/SiC interface provides a strong thermodynamic driving force for 2D films to form. Researchers reported films down to a few atomic layers thick in both works. Cross-sectional transmission electron microscopy (TEM) images reveal the high crystallinity and well-controlled thickness of the grown film. In summary, CHet is an excellent approach to prepare wafer-scale ultrathin non vdW 2D materials, although the achievable products are limited by the availability of precursors and substrates. The as-grown films is also difficult to be transferred to another substrate for post processing, as the films are tightly bonded with the growth substrate.[128]

Liquid metal printing

Liquid metal printing is an emerging method to synthesize non-layered 2D metal oxides.[97,129–131] Liquid metals, referring to those whose melting points are close to or below room temperature (*e.g.*, Ga, In, Hg), are ideal hosts for 2D metal oxides due to their electron-rich bulk and abundant interfaces with surrounding environments. When exposed to an oxygen-rich atmosphere, an ultra-thin oxide skin forms at the surface of liquid metal driven by its chemical active characteristics.[116] Such oxide skin can be easily isolated from the parent liquid metal and transferred onto an arbitrary substrate. Two main techniques are used to separate the 2D metal oxide skin from the parent liquid metal.[61] The first is a straightforward peeling method by touching the liquid metal droplet with a substrate (*e.g.*, SiO_2/Si). The oxide skins usually possess weak interactions with the liquid metal but a strong interaction with the substrates, which facilitates the peeling-off. Another technique is

the gas injection method in which compressed air is injected to the liquid metal, causing the ultrathin oxide layer to form rapidly at the air bubble interface. Afterwards, the oxide skin will be dispersed into the DI water surrounding the liquid metal droplet, then the products can be further collected through drop-casting onto the substrate. Using the liquid metal printing strategy, Zavabeti *et al.* obtained several non-layered 2D metal oxides such as Ga_2O_3, HfO_2, Al_2O_3, and Gd_2O_3 (Figure 2d),[61] all of which show smooth surfaces with ultrathin thickness from 0.51 nm to 2.78 nm. It is worth mentioning that the HfO_2 film obtained from gas injection featured an amorphous structure, while the peeling method gives polycrystalline oxides, which is attributed to rapid growth within a shorter reaction time frame in the injection technique.

The liquid metal printing technique shows great capability for wafer-scale synthesis of 2D metal oxide films with low thermal budget, which is in great demand for integrating 2D materials with existing CMOS technologies.[132–134] The printed 2D metal oxide film can be used as templates to synthesize other 2D materials as well. For instance, Syed *et al.* further converted printed 2D Ga_2O_3 into amorphous 2D GaN.[131] Nevertheless, this method usually produces samples with short-range crystallinity, and the uniformity of the film thickness is dominated by the surface oxidation and difficult to control. Moreover, the number of 2D materials achievable using this method is also restricted by the limited number of metals with low melting points.

Atomic substitution

Very recently, a surface-confined atomic substitution approach that combines the ease of downscaling vdW materials and chemical reactions has been demonstrated to obtain ultra-thin non vdW 2D materials.[57–59,78,135] VdW materials such as MoS_2 are first exfoliated into 2D flakes as the precursor, then a chemical reaction is applied to convert them into the 2D flake of a non vdW material. The converted non vdW 2D flakes inherit the morphology and 2D nature from their vdW

2D precursors. Figure 2e presents the schematic illustration and examples of this approach. Cao *et al.* performed the nitridation reaction on MoS_2 flakes and obtained non vdW Mo_5N_6 flakes (thickness down to 2.1 nm) with inherited morphology and crystalli nity.[78] Thickness of the obtained Mo_5N_6 decreases to 40% of the original thickness of the MoS_2 precursor due to the vanish of the vdW gaps.[78] They also notice that the conversion works the best for MoS_2 flakes with the thickness in the range of 5 to 15 nm (2 to 6 nm in term of Mo_5N_6). They further demonstrated that this approach could be applied to make other non vdW metal nitrides, such as W_5N_6, TiN and GaN by converting the vdW WS_2, TiS_2 and GaS, respectively.[78,79] In this process, the metal skeleton remains and chalcogen atoms are liberated from the lattice under high temperature (600-800 °C), followed by the formation of metal-nitrogen bonds in the NH_3 atmosphere.[78,79,86] Li *et al.* further showed that the conversion initiates from both the edge and the defect sites on the surface of a precursor flake, followed by an epitaxial conversion process.[136,137] The converted nitride crystals are observed to share the same crystal orientation as the MoS_2 precursor flakes.

There are several advantages of this approach toward providing non vdW 2D materials: (1) the thickness of the obtained non vdW 2D materials can be precisely controlled and tuned by the number of layers of the vdW 2D precursor;[78] (2) Heterostructures between the converted non vdW material and the vdW precursor material can be realized readily through the partial conversion. Examples are discussed in later section (Fabrication of high-quality heterostructures); (3) This method can be extended to synthesize many other non vdW 2D materials by using different vdw materials as precursors and carrying out different chemical reactions. For example, a few chemical reactions have been exploited in preparing the 2D form of the non vdW crystals from corresponding vdW 2D precursors: $MoS_2 + CH_4 \rightarrow Mo_2C$,[135,138] $InSe + XeF_2 \rightarrow InF_3$,[59] $CdI_2 + S \rightarrow CdS$,[58] $MoS_2 + PH_3 \rightarrow MoP$,[57] and $HfS_2 + O_2 \rightarrow HfO_2$.[89] In all these cases, non vdW 2D flakes

with their thicknesses ranging from few nanometers to tens of nanometers with smooth surfaces were reported. Additionally, the thickness of the synthesized non vdW flakes substantially reduces compared to the vdW precursors, aligning with the disappearance of vdW gaps in the crystals. On the negative side, products of the atomic substitution method are limited by the availability of precursors in their 2D forms. Synthesis of single-atom-thick flakes has not been achieved either. As reported by Wang *et al.*, the conversion from MoS_2 to MoP produces amorphous film if monolayer MoS_2 flakes are used as precursors.[57] Crystalline areas are observed in thicker samples and the portion of crystalline area increases with thickness of the precursor MoS_2 flakes.

Properties modification at 2D limit

It has been widely reported that vdW 2D materials often undergo significant property changes compared to their bulk counterparts due to the quantum confinement effect, disrupted structural symmetry, and increased specific surface area (SSA).[1,48,49,139–147] For example, the optical bandgap energy of MoS_2 increases from 1.2 eV (bulk) to 1.8 eV (monolayer) and transit from an indirect to a direct bandgap.[18,45] The dimension-controlled properties are also expected in non vdW materials. However, due to the lack of available samples, there are only a handful of studies reported this phenomenon. Below are several instances of reported property modifications for non vdW materials at the 2D limit compared to their bulk counterparts, where the quantum confinement effect and increased SSA play key roles. We expect the discussion on these studies to serve as potential inspirations for further research in the field.

Notably enlarged bandgap energies have been reported in some non vdW wide gap semiconductors at the 2D limit. Group III-V compounds, especially GaN, has been widely studied conventionally for optoelectronic applications due to its wide, direct bandgap (3.4 eV), high electrical breakdown voltage, and high charge carrier mobilities.[148] As shown in Figure 3a,

calculations have predicted that the bandgap energy would increase dramatically at reduced thicknesses from ~ 4 eV for a 5-layer sample to 5.28 eV for a monolayer sample.[127] With the increase of bandgap energies, the performance of GaN-based optoelectronic devices is expected to be further improved due to the enhanced excitonic effect at larger band gaps.[149,150] Experimental observations also echo with the theoretical predictions. Chen *et al.* reported that GaN single crystals exhibit prominent blue-shift from bulk to 2D in photoluminescence emission spectra, as shown in Figure 3b, where the emission peak shifts from 3.40 eV (bulk) to 3.76 eV (5.2 nm).[90] A stronger emission intensity is also observed on 2D GaN flakes, which is attributed to a higher internal quantum efficiency at reduced dimension. Cao *et al.* also reported the blue shift of photoluminescence emission in 2D GaN with sample thicknesses, where the emission peak shifts from 3.5 eV (25 nm thick) to 3.7 eV (4.4 nm thick).[79]

In addition to the modulation of bandgap energies, recent investigations have unveiled a noteworthy reversal in the magnetic ordering of α-Fe_2O_3 as it undergoes dimensional reduction from bulk (hematite) to a 2D form known as hematene.[84,114] Extensive studies have traditionally classified hematite as a weak ferromagnetic (FM) material above the Morin transition temperature (T_M) of approximately 265 K, transitioning into an antiferromagnetic (AFM) state below T_M.[151] Interestingly, Balan *et al.* studied hematene with thickness down to 0.8 nm, revealing consistent FM properties across the entire temperature range from 10 K to 300 K.[114] Figure 3c and 3d show the field cooled-zero field cooled (FC-ZFC) curves of hematite and hematene, respectively. The differential of the curves is shown in the insets, where a sharp peak in the hematite suggests an abrupt transition from FM to AFM around T_M. Meanwhile, no such transitions were observed for hematene. The distinctive magnetic ordering exhibited by hematene is attributed to an increased influence of surface spins at lower dimensions. In α-Fe_2O_3, the Fe^{3+}-O-Fe^{3+} superexchange

interactions contribute to the AFM ordering, but the magnetic moment associated with this interaction is markedly reduced at the surface.[152] The elevated SSA at the 2D limit suppresses AFM ordering in hematene, leading to its manifestation of FM ordering.

Advancing the 2D electronics as key components

With the persistent exploration of 2D materials, researchers have discovered many materials with promising electrical and optical properties that can advance the development of flexible and ultrascaled electronics.[5,32,33,112,153] Field-effect transistors (FETs) are the building blocks of electronic devices such as logic gates, current amplifiers, and electronic oscillators. A FET typically consists of three components, *i.e.*, metallic contacts, insulating dielectrics, and semiconducting channels.[20] Each of these components plays a specific role in the operation and hence different figures of merit are developed to benchmark the candidate materials for each part.[154,155] In the semiconductor channels, the charge carrier (electrons or holes) mobility is one of the critical properties, as this quantity determines how fast the FETs channel responds to gate tuning, and hence the switching speed of the FETs. For dielectric materials, conversely, the dielectric constant (k) and dielectric strength (*i.e.* breakdown electric field intensity) are the key material metrics, as the gate tunability relies on these parameters. Hereby, we will discuss the recent progress of non vdW 2D materials in achieving semiconductors with high charge carrier mobility and dielectrics with high dielectric constants, which are valuable supplements to 2D electronics due to their rarity among vdW 2D materials.

<u>High mobility semiconductors</u>

TMDs are widely studied and especially as semiconducting channel materials in FETs due to their appropriate bandgap energies, and have been well recognized as promising candidates for beyond-

silicon technologies.[18,156,157] Despite that the charge carrier mobility in bulk MoS_2 is typically over an order of magnitude lower than that of single crystalline Si films, the situation reverses at the 2D limit.[42,48–50] Monolayer MoS_2 has much higher mobility values than Si of similar thicknesses as charge carriers experience significant scattering in ultrathin (< 3 nm) Si due to the rough surface and surface dangling bonds.[42] However, although surface dangling bonds are the nature of non vdW materials, it is rational to expect that improved synthesis techniques will produce a smooth surface and reduce scatterings. Aiming on this task, researchers have been attempting to prepare high-quality conventional semiconductors (*e.g.*, GaN and Ge) in their 2D form through CVD approaches.[90,94] Figure 4a shows the schematic illustration and false-colored SEM image of a back-gated FET device made on a GaN flake. The transfer curve in Figure 4c shows an n-type semiconducting behavior of 2D GaN with a field effect mobility of 160 $cm^2 V^{-1} s^{-1}$.[90] In the case of 2D Ge, Hu *et al.* reported a hole mobility of 263 $cm^2 V^{-1} s^{-1}$ on a ~20 nm thick sample.[94] It is worth noting that the sample thicknesses in these works far exceed the thickness of monolayer MoS_2, so the direct comparison of mobility values would not be fair. Yet they provide a promising starting point for future research.

High-k dielectrics

Apart from channel semiconductors, insulating materials are another critical constituent in modern electronic chips as gate dielectrics, insulating spacers, and thermal dissipation materials.[158] Different criteria are applied to evaluate candidate materials for each application, and we will focus on gate dielectrics in the discussion within this section. For gate dielectrics, a high k value is essential for the effective tuning of FETs. Unfortunately, preparing vdW 2D materials with high k is still a great challenge in the field after two decades of exploration. The most commonly used vdW 2D dielectrics, hBN, has a k value of 3~5, which is comparable to the thermal oxide SiO_2.[159]

In fact, hBN is not the best candidate for dielectrics if considering its dielectric constant. Plenty of dielectric materials with much higher k values than hBN have been discovered,[56] although scaling down these materials into 2D regime is a challenging task due to their non vdW crystal structure.

In recent years, the synthesis of non vdW 2D Ta_2O_5 and HfO_2 through an oxidation process of the corresponding 2D sulfide flakes has been reported.[83,87–89,92] Owing to the unstable structure and a consequential low oxidation threshold, HfS_2 and TaS_2 can be easily oxidized through oxygen plasma exposure,[83,89] laser irradiation,[92] or thermal annealing in air.[87,88] Very recently in 2022, Huang *et al.* and Yang *et al.* reported the scale down of another non vdW material with an ultra-high k value, $SrTiO_3$, into the 2D form through an epitaxial growth process.[93,160] The dielectric constant of the synthesized layer increases with thickness, while a maximum value around 100 was observed at 30 nm thickness, which is around thirty times higher than hBN.[159] Hereby, we summarize the k values and dielectric strengths of 2D $SrTiO_3$,[93,160] HfO_2,[83,89] Ta_2O_5,[87,88] and compare with hBN in Figure 5.[158,161–164] Apart from k values, we also compared the equivalent oxide thickness (EOT) of each tested film in the inset of Figure 5a. EOT describes the equivalent thickness of SiO_2 required to match the specific capacitance of the tested film, and it is given by the formula $EOT = \frac{k_{SiO_2}}{k_x} \cdot t_x$. Here k_{SiO_2} and k_x are the dielectric constant of SiO_2 and tested film, respectively, and t_x is the thickness of the tested film. Note that a lower EOT value at the same film thickness suggests more efficient gate tuning. From Figure 5a, the non vdW metal oxides show much higher k values than hBN, which is beneficial for high-performance FETs.

Fabrication of high-quality heterostructures

2D heterostructures have been extensively studied and demonstrated great promises in electronic devices applications. Summarizing from research over a decade, a common sense has recently

been established that a chemically clean, atomically sharp, and well contacted interface is vitally important for high performance devices.[3,165,166] Artifacts generated during the fabrication process usually leads to degradation of device performance. For example, the conventional approach to fabricate electrodes on 2D materials (lithography and metal deposition) usually introduces polymer residue at the metal-semiconductor interface (from lithography) and chalcogen vacancies in TMDs (during metal deposition).[51,52,167,168] Such contaminated interface inevitably leads to the FLP effect, which raises the Schottky barrier height for charge transport, resulting in high contact resistances, and low charge carrier mobilities.[52,169] Another example is excess contamination introduced during the fabrication process of vdW heterostructures (*e.g.*, h-BN/TMDs heterostructures) by transferring and stacking. The air bubble and polymer residues deteriorate the interaction between two 2D layers at the interface.[3,165,170,171]

Recent advancements in the synthesis of non vdW 2D materials, especially through atomic substitution, have enabled a technical route for fabricating high-quality 2D heterostructures. This approach involves converting vdW 2D materials into their non vdW counterparts in a selective and controllable manner. Both lateral (parallel to the vdW gap) and vertical (across the vdW gap) heterostructures have been achieved *via* rational design (Figure 6a and 6b): Li *et al.* fabricated MoS_2-MoN lateral heterostructures by encapsulating part of a MoS_2 flake and converting the exposed region into MoN;[136] Lai *et al.* treat multilayer HfS_2 with O_2 plasma and converted the surface layers into HfO_2 to form HfS_2-HfO_2 vertical heterostructures.[89] The sample degradation and contamination are minimized by avoiding the use of polymer and exposure of the sensitive surfaces. In this section, we will introduce some recent studies on achieving a clean and sharp interface using vdW-non vdW 2D heterostructures and the consequential performance

improvement. These heterostructures have been reported to use as (1) metal-semiconductor edge contacts, and (2) native oxide insulating layer on 2D semiconductors.

Metal-semiconductor edge contact

Compared to surface contacts, the edge contact geometry shows the capability to improve the metal-semiconductor contacts for vdW 2D materials.[44,172] Higher charge carrier mobility and lower contact resistance have been reported in MoS_2- and graphene-based FETs with edge contacts.[44,172,173] However, fabricating this lateral heterostructure with high quality interface is difficult with conventional fabrication techniques. The process involves patterning the flakes with polymers followed by plasma etching and metal deposition, where polymer residues, over-etching, and edge exposure inevitably degrades the connection between 2D flakes and metal electrodes.[172] Li *et al.* demonstrated an alternative approach to fabricate the edge contact by converting the two ends of a MoS_2 flake into MoN with NH_3, while the middle is passivated by an Al_2O_3 mask (Figure 6a).[136] The obtained MoN-MoS_2-MoN structure is a metal-semiconductor-metal heterojunction with atomically bonded seamless one-dimensional (1D) interfaces. In another work, Jeon *et al.* reported a MoS_2-Mo_2C lateral heterostructure fabricated using a similar method, where CH_4 instead of NH_3 is used for the conversion for Mo_2C.[135,138] Reduced contact resistances and lower Schottky barrier heights are observed in both works compared to conventional top metal electrodes.[51,136,173] Planar high resolution TEM images confirmed clean and atomically sharp interfaces across the MoS_2-MoN junction (Figure 6c-f), which facilitates the transport of charge carriers.[44] Although Schottky contacts are still observed at the interface in these works, we envision that the ultimate Ohmic contact can be realized by engineering the band alignment between the semiconductor and metallic material in this lateral heterostructure. For example,

partially converting MoS_2 into another metallic material whose work function matches the electron affinity of MoS_2 will lead to an ideal contact to n-type channel.[173]

Native oxide insulating layer

Atomic layer deposition (ALD) is a powerful technique to prepare a variety of metal oxide films (*e.g.*, HfO_2) as dielectric layers for Si technologies.[158] However, when adapted to TMDs devices, the uniformity of the deposited film experience serious degradation attributed to the hydrophobic nature of TMDs surfaces.[174–176] In response to this technical obstacle, Lai *et al.* demonstrated a method to construct HfS_2-HfO_2 vertical heterostructures.[89] This involves treating HfS_2 flakes with O_2 plasma to convert surface layers into HfO_2, and subsequently depositing gate electrodes (Figure 6b). In this context, the native HfO_2 layer functions as a dielectric for the HfS_2 channel. Cross-sectional scanning transmission electron microscopy (STEM) measurements validate the uniform HfO_2 layer and atomically sharp interface in this HfS_2-HfO_2 heterostructure (see Figure 6g and 6h), representing a substantial improvement compared to the analogues prepared through ALD routes. Notably, a reported subthreshold swing (SS) value of ~67 mV/dec establishes a benchmark for 2D HfS_2-based FETs. Furthermore, thickness of the oxide layer can be controlled by carefully tuning the plasma processing parameters. Borah *et al.* demonstrated the conversion of topmost layer of few-layer WSe_2 flakes into an ultra-thin tungsten oxyselenide (TOS) tunneling layer for the metal-insulator-semiconductor (MIS) contact strategy.[177] The application of the TOS tunneling layer imposes a significant improvement in performance compared to conventional WSe_2 FETs. To sum up, the atomic substitution approach provides a great way to fabricate high-quality 2D heterostructures, which is vital for electronic devices applications.

Conclusion and future directions

In summary, non vdW 2D materials exhibits substantial promise as key components in 2D electronic devices. Due to the challenges in synthesis, the study of non vdW 2D materials is still in the early stages compared to the vdW 2D field and there are ample opportunities for future investigations. Nonetheless, numerous studies have emerged, underscoring the considerable potential of non vdW 2D materials as valuable additions to vdW 2D materials and beyond. Anticipated to play a pivotal role in advancing 2D electronic devices toward practical applications, non vdW 2D materials hold significant promise. Here, we present our insights into future directions that merit attention to expedite the development of non vdW 2D materials, with the aim of inspiring researchers engaged in this field.

(1) Explore more non vdW 2D materials. The rapid advancement of vdW 2D materials in the past two decades has propelled the evolution of nanoelectronics,[32,33,178] while the study of non vdW 2D materials already shows potential in filling the gaps in vdW 2D materials, fostering materials evolution. Although the synthesis method and properties of quite a few non vdW 2D materials have been reported, there remains ample space for exploration along this path. Exploring the downscaling of more non vdW crystals will be the essential task to search for desired properties and functionalities. We suggest that future studies should focus on scaling down the non vdW materials whose bulk phases already show great properties or are commercialized for industrial applications, such as III-V semiconductors and their alloys.[148,179] We also want to point out that at the early stage, achieving successful synthesis and understanding the fundamental properties of the material is more important than other practical considerations (*e.g.*, harsh synthesis conditions).

(2) Synthesis of single-unit-cell non vdW 2D materials. Despite various demonstrated synthesis routes for non vdW 2D materials, the majority of synthesized films and flakes are composed of multiple unit cells with thickness ranging from a few to tens of nanometers.[105,110]

Materials with thickness of a single unit cell, representing the thinnest limit of the interested non vdW materials, have rarely been reported. This is a rather challenging task owing to the strong interlayer bonding in non vdW crystals. Yet, realizing single-unit-cell layers would provide access to many fascinating phenomena considering that the quantum confinement effect is maximized at this limit.[18] It could also potentially create an unexplored set of 2D crystals that are distinct from the common phases existing in bulk, boosting the discovery of more functionalities.

(3) Scalable synthesis. Apart from the downscaling of crystals, it is also crucial to upscale the lateral size of the 2D material for practical applications (integrated circuits, *etc*.). The isotropic strong bonding in non vdW crystals facilitates the growth in all dimensions, restricting the domain size of the ultra-thin 2D crystals. This limitation results in small lateral size of the crystals or excessive domain boundaries in a continuous film. While some experimental approaches, like liquid metal printing, have achieved wafer-scale non vdW 2D films, this method may not provide access to many highly crystalline 2D crystals.[97] Therefore, achieving scalable synthesis of 2D non vdW crystals is imperative for their industrial applications.

(4) Property modifications through surface termination group engineering. Different from the saturated surface of vdW 2D materials, non vdW 2D materials possess a surface rich of dangling bonds. The unsaturated surface is in a metastable state and can bind with functional groups from the external environment.[180] We consider the dangling-bond-rich surface as a double-edge sword: On the negative side, the random termination groups on the surface of the non vdW 2D materials could cause the deviation and a variation of their properties. On the positive side, it offers a potential avenue to tune and control the properties of the non vdW 2D materials. Learning from the extensively studied MXenes materials, which also possess dangling-bond-rich surfaces, the work function and adsorption energy of gas molecules can be tuned through engineering the

surface termination groups.[181,182] While controlling, tuning and characterizing termination group engineering remains largely unexplored for most non vdW 2D materials, we envision this as a promising direction to advance this research field.

(5) Doping techniques for p- and n-type semiconductors. Envisioning the discovery of a variety of semiconducting non vdW 2D materials with desired properties for nanoelectronics in the next decade, a few more process nodes for this group of materials are to be developed to enhance their industrial applications. Both p- and n-type doping techniques are to be developed for the fabrication of high-performance FETs devices with non vdW 2D semiconductor channels. Similar to vdW 2D materials, many doping techniques designed for bulk crystals (*e.g.*, ion implantation) will not be applicable to non vdW 2D materials, especially the ultrathin ones, due to the excess strain and defects induced during the process.[5] Substitutional doping, either during or after the synthesis process, is highly preferred to achieve stable and effective material tuning.

Acknowledgments

This work is supported by the U.S. Department of Energy (DOE), Office of Science, Basic Energy Science (BES) under Award Number DE-SC0021064. X.L. acknowledges the membership of the Photonics Center at Boston University. H. G. acknowledges the support of BUnano fellowship from Boston University Nanotechnology Innovation Center. Work done by X.L. is also supported by the National Science Foundation (NSF) under Grant No. 1945364.

Figures

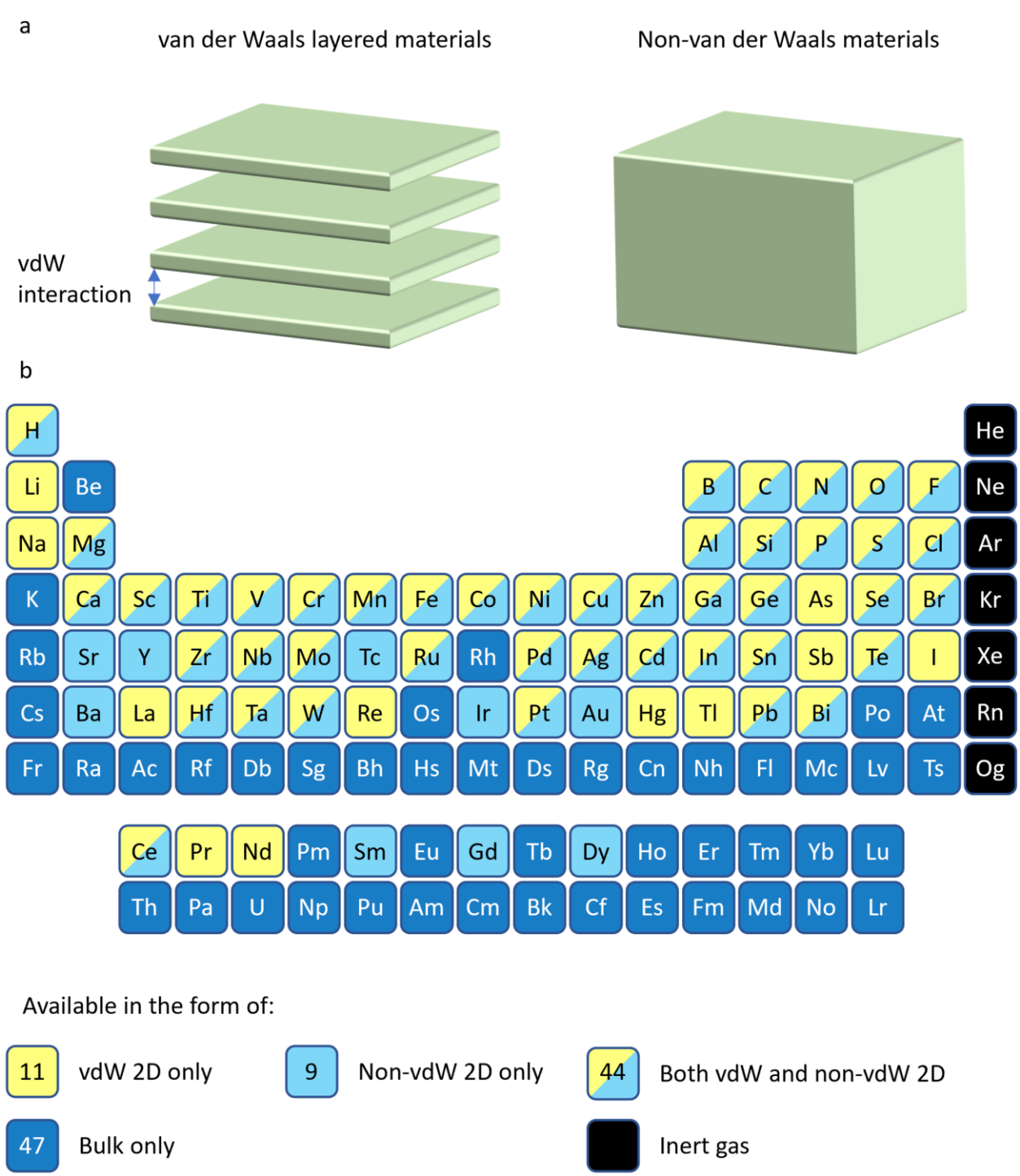

Figure 1 (a) Schematic illustration of van der Waals crystals and non-van der Waals crystals. (b) Periodic table summarizing the elements present in 2D and bulk forms.

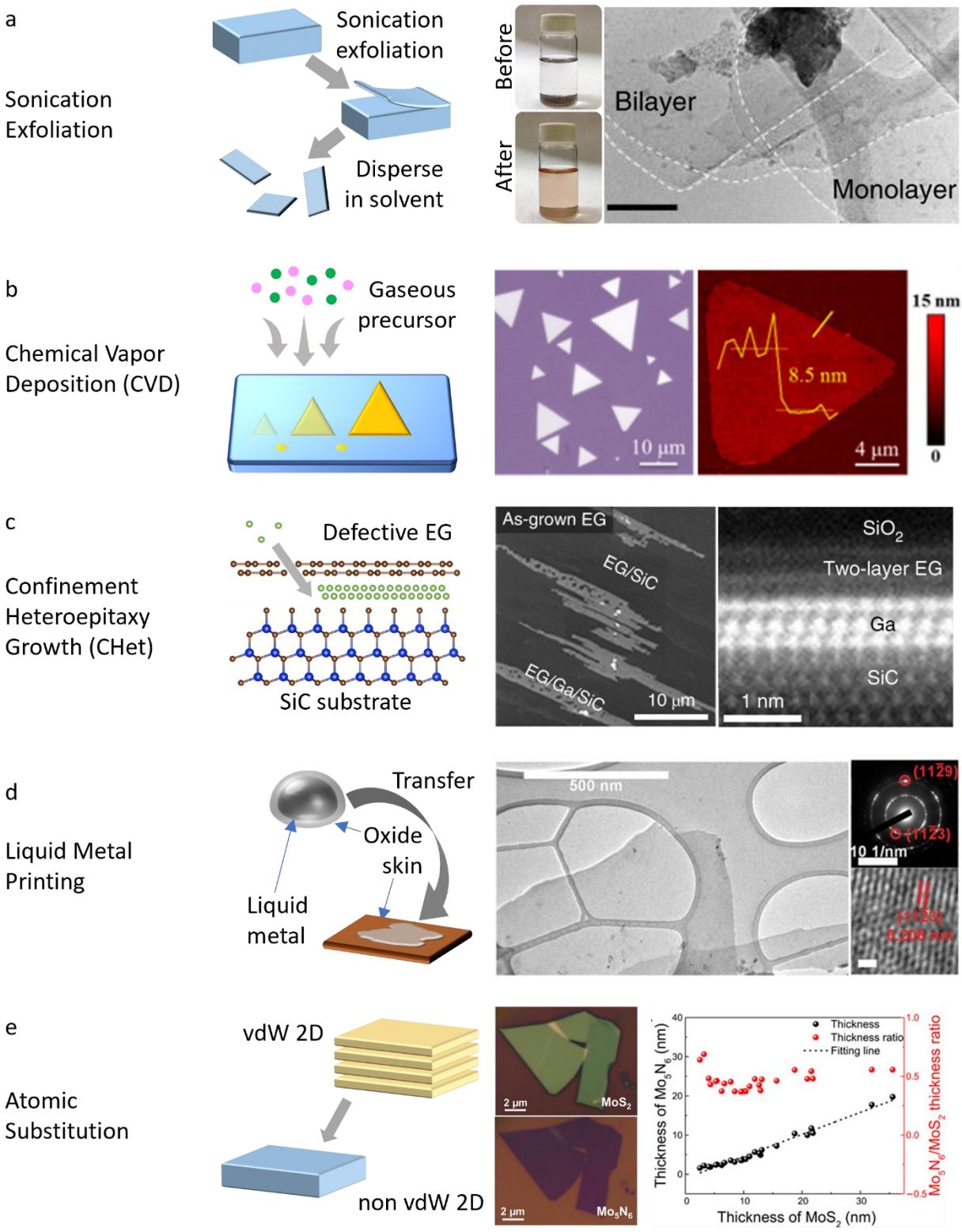

Figure 2 Schematic drawing and representative results of synthesis approaches for non vdW 2D materials.

Figure 2 cont. (a) Sonication exfoliation. Optical images show the bulk and 2D α-Fe_2O_3 dispersed in DMF. SEM image shows the exfoliated monolayer and bilayer α-Fe_2O_3.[114] Image was reproduced with permission from Ref. 114. Copyright 2018 Springer Nature. (b) Chemical vapor deposition (CVD). Optical and AFM images of synthesized Ge flakes show their 2D nature.[94] Image was reproduced with permission from Ref. 94. Copyright 2018 American Chemical Society. (c) Confinement heteroepitaxy growth (CHet). SEM and cross-sectional TEM images of 2D Ga film are presented.[128] Image was reproduced with permission from Ref. 128. Copyright 2020 Springer Nature. (d) Liquid metal printing. SEM, TEM and SAED of the prepared Al_2O_3 film reveal polycrystallinity in the sample.[61] Image was reproduced with permission from Ref. 61. Copyright 2017. Copyright American Association for the Advancement of Science. (e) Atomic substitution. Optical images show observable change after reaction. Thickness of the flakes decreased significantly from AFM measurements.[78]

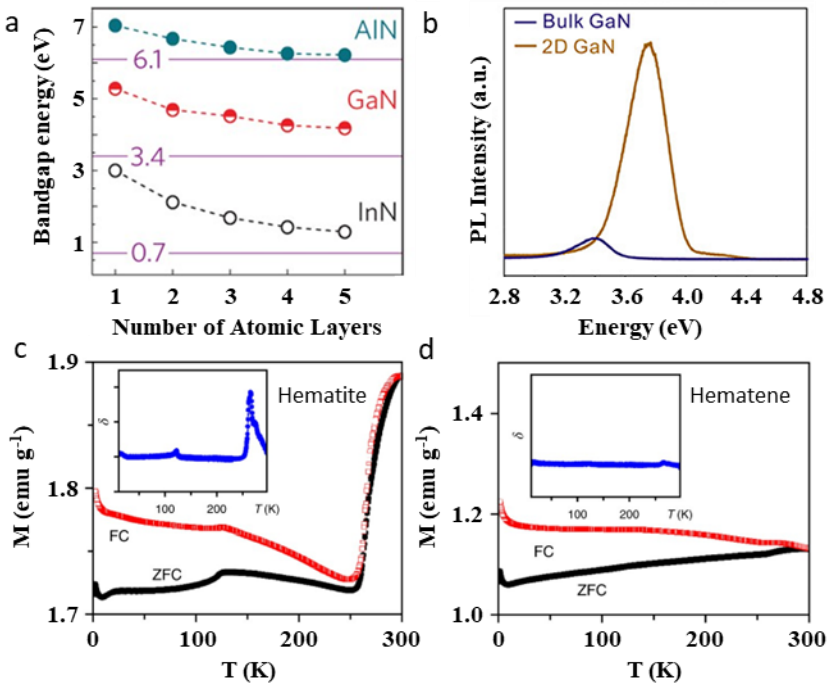

Figure 3 Properties modification of non vdW materials at 2D limit. (a) Calculated thickness dependence of bandgap energy of different III-V compounds.[127] Image was reproduced with permission from Ref. 127. Copyright 2016 Springer Nature. (b) Photoluminescence spectra of bulk and 2D GaN.[90] Image was reproduced with permission from Ref. 90. Copyright 2018 American Chemical Society. (c, d) FC-ZFC plot of hematite (c) and hematene (d).[114] Insets show the derivatives of the corresponding plots. Image was reproduced with permission from Ref. 114. Copyright 2018 Springer Nature.

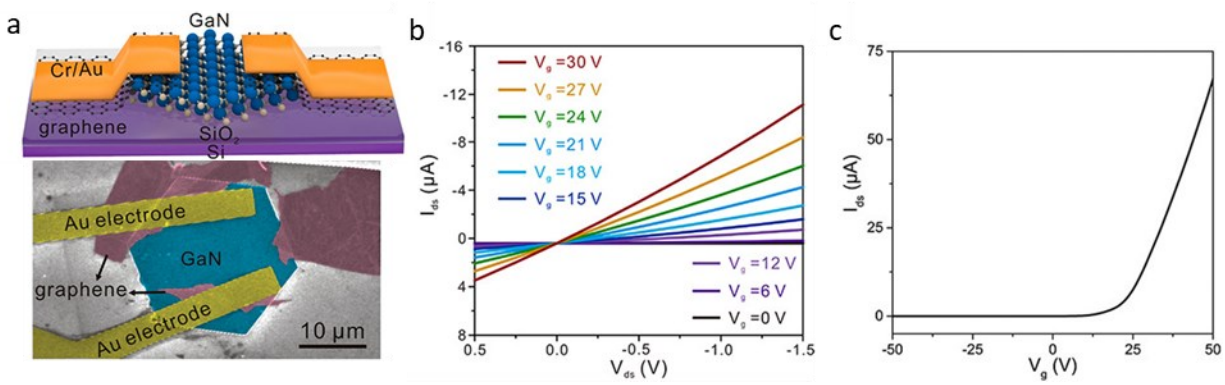

Figure 4 High mobility semiconductors. (a) Schematic and false-colored SEM image of GaN FETs device. (b) Transport measurements of 2D GaN. (c) Transfer curve of 2D GaN.[90] Image was reproduced with permission from Ref. 90. Copyright 2018 American Chemical Society.

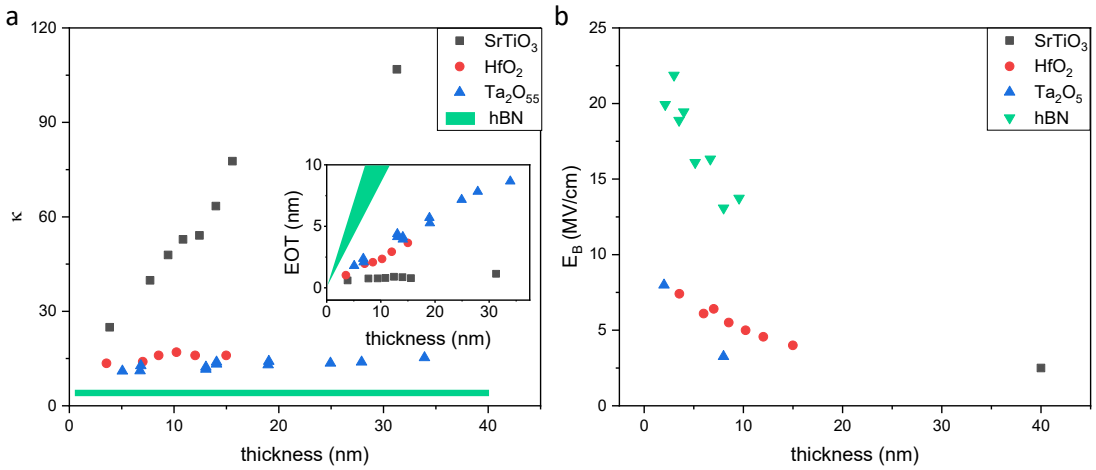

Figure 5 High-k dielectrics. (a) Dielectric constant (k) of each material at different thicknesses. Inset shows the EOT of each data point. (b) Dielectric strength (E_B) of each material at different thicknesses.

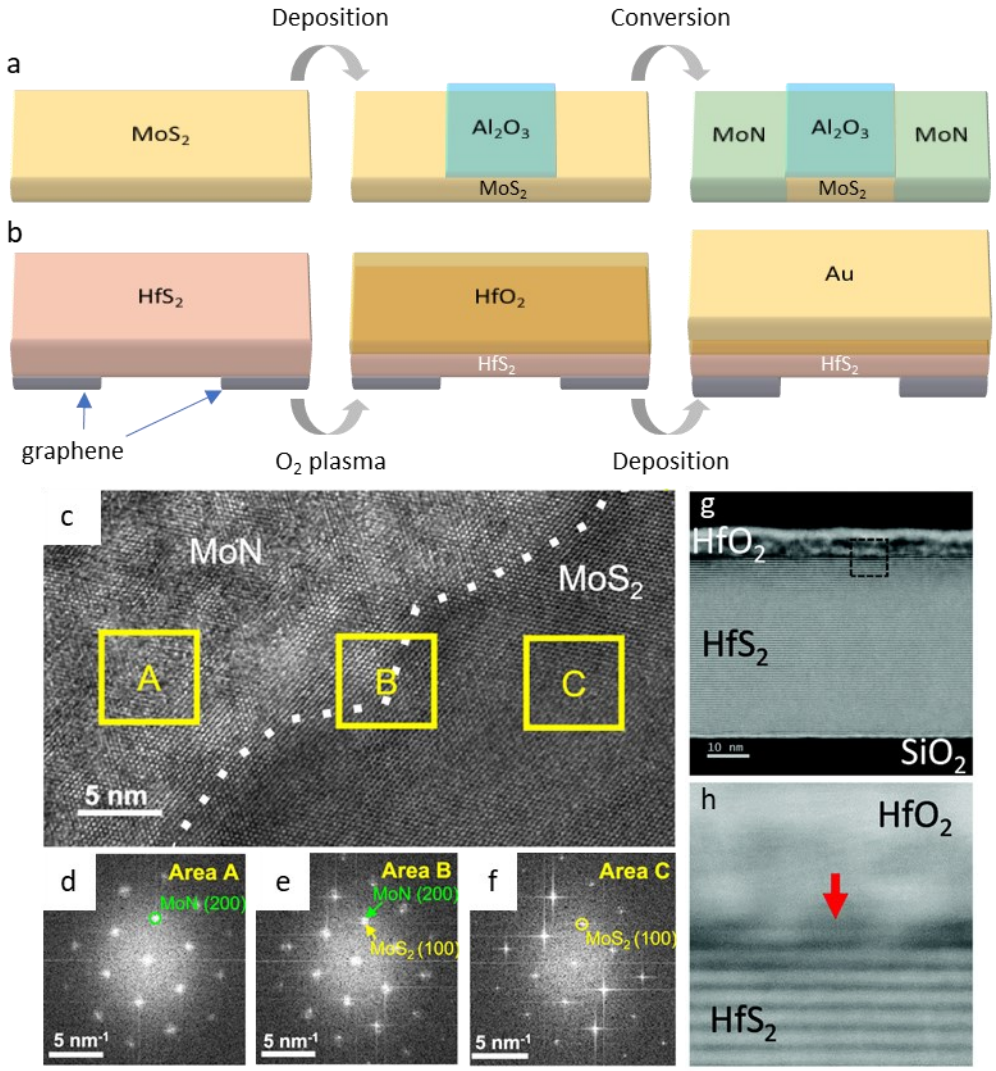

Figure 6 Fabrication of vdW/non vdW heterostructures through atomic substitution. (a, b) Schematic illustration of fabrication process for lateral (a) and vertical (b) heterostructures. (c-f) High resolution planar TEM image (c) and fast Fourier transformation (FFT) patterns (d-f) of each section in the MoS_2-MoN lateral heterostructure: (d) MoN, (e) interface, (f) MoS_2.[136] Images were reproduced with permission from Ref. 136. Copyright 2022 American Chemical Society. (g, h) High resolution cross-sectional STEM image HfS_2-HfO_2 vertical heterostructure. (h) shows the zoom-in image of area labeled with black square in (g).[89] Inages were reproduced with permission from Ref. 89. Copyright 2018 Royal Society of Chemistry.

Table 1 Representative vdW and non vdW 2D materials achieved experimentally for each element.

Atomic number	Element	vdW 2D	Non vdW 2D	Atomic number	Element	vdW 2D	Non vdW 2D
1	H	$Mg(OH)_2$	$Al(OH)_3$	43	Tc	N/A	TcN
2	He	Inert gas		44	Ru	$RuCl_3$	RuO_2
3	Li	Li_xCoO_2	N/A	45	Rh	N/A	N/A
4	Be	N/A	N/A	46	Pd	$PdSe_2$	Pd film
5	B	h-BN	MoB_2	47	Ag	$AgCrP_2Se_6$	Ag film
6	C	Graphene	Mo_2C	48	Cd	$CdPS_3$	CdS
7	N	h-BN	Mo_5N_6	49	In	InSe	InF_3
8	O	MoO_3	TiO_2	50	Sn	$PbSnS_2$	Sn film
9	F	Fluorographene	InF_3	51	Sb	Sb_2S_3	N/A
10	Ne	Inert gas		52	Te	WTe_2	Cr_2Te_3
11	Na	$Na_2Co_2TeO_6$	N/A	53	I	CrI_3	N/A
12	Mg	$MgPS_3$	$Mg_3(PO_4)_2$	54	Xe	Inert gas	
13	Al	Al_2SiO_5	Al_2O_3	55	Cs	N/A	N/A
14	Si	Al_2SiO_5	Zn_2SiO_4	56	Ba	N/A	Ba_2ClF_3
15	P	Black P	MoP	57	La	$LaTe_2$	N/A
16	S	MoS_2	CdS	58	Ce	CeF_3	CeO_2
17	Cl	$RuCl_3$	AgCl	59	Pr	PrF_3	N/A
18	Ar	Inert gas		60	Nd	NdF_3	N/A
19	K	N/A	N/A	61	Pm	N/A	N/A
20	Ca	$Ca(OH)_2$	$CaCO_3$	62	Sm	N/A	SmF_3
21	Sc	$AgScP_2S_6$	AlScN	63	Eu	N/A	N/A
22	Ti	TiS_2	TiO_2	64	Gd	N/A	Gd_2O_3
23	V	VS_2	V_2N	65	Tb	N/A	N/A
24	Cr	$CrPS_3$	CrN	66	Dy	N/A	Dy_2S_3
25	Mn	MnP_2S_6	MnO_2	67	Ho	N/A	N/A
26	Fe	$FePS_3$	FeS	68	Er	N/A	N/A
27	Co	$CoPS_3$	CoO	69	Tm	N/A	N/A
28	Ni	$NiPS_3$	NiO	70	Yb	N/A	N/A
29	Cu	$CuPSe_3$	CuBr	71	Lu	N/A	N/A
30	Zn	$ZnPS_3$	ZnS	72	Hf	HfS_2	HfO_2
31	Ga	GaS	GaN	73	Ta	TaS_2	Ta_2O_5
32	Ge	GeSe	Ge	74	W	WS_2	W_5N_6
33	As	As_2S_3	N/A	75	Re	ReS_2	N/A
34	Se	WSe_2	Cr_2Se_3	76	Os	N/A	N/A
35	Br	$TiBr_3$	CuBr	77	Ir	N/A	$SrIrO_3$
36	Kr	Inert gas		78	Pt	$PtSe_2$	Pt film
37	Rb	N/A	N/A	79	Au	N/A	Au film
38	Sr	N/A	$SrTiO_3$	80	Hg	$Hg_2P_2S_6$	N/A
39	Y	N/A	YBa_2CuO_x	81	Tl	$TlGaS_2$	N/A
40	Zr	ZrS_2	ZrN	82	Pb	$PbSnS_2$	$CH_3NH_3PbI_3$
41	Nb	NbS_2	NbN	83	Bi	Bi_2Te_3	$CuBi_2O_4$
42	Mo	MoS_2	Mo_2C	84	Po	N/A	N/A

Table 1 Cont.

Atomic number	Element	vdW 2D	Non vdW 2D
85	At	N/A	N/A
86	Rn	Inert gas	
87	Fr	N/A	N/A
88	Ra	N/A	N/A
89	Ac	N/A	N/A
90	Th	N/A	N/A
91	Pa	N/A	N/A
92	U	N/A	N/A
93	Np	N/A	N/A
94	Pu	N/A	N/A
95	Am	N/A	N/A
96	Cm	N/A	N/A
97	Bk	N/A	N/A
98	Cf	N/A	N/A
99	Es	N/A	N/A
100	Fm	N/A	N/A
101	Md	N/A	N/A
102	No	N/A	N/A
103	Lr	N/A	N/A
104	Rf	N/A	N/A
105	Db	N/A	N/A
106	Sg	N/A	N/A
107	Bh	N/A	N/A
108	Hs	N/A	N/A
109	Mt	N/A	N/A
110	Ds	N/A	N/A
111	Rg	N/A	N/A
112	Cn	N/A	N/A
113	Nh	N/A	N/A
114	Fl	N/A	N/A
115	Mc	N/A	N/A
116	Lv	N/A	N/A
117	Ts	N/A	N/A
118	Og	Inert gas	

Table 2 Non vdW 2D materials reported for nanoelectronics and optoelectronics applications

Material	E_g (eV)	Thickness (nm)	Lateral size (μm)	Highlights
Cr_2S_3[95]	-	1.9-7.9	~150	p-type, T_N = 120 K
Fe_3O_4[96]	0.038-0.057	4-40	4-7	Broadband photodetection up to 10.6 μm
Fe_2O_3[114]	2.7	1-4	~20	Ferromagnetic hysteresis loop
CdS[58]	-	2-35	~100	Fast photodetection rise & decay (50 μs)
GaN[90]	3.76	~4	~20	Mobility = 160 $cm^2 \cdot V^{-1} \cdot s^{-1}$, on/off ~ 10^6
Ge[94]	0.67	8-25	~20	Mobility = 263 $cm^2 \cdot V^{-1} \cdot s^{-1}$
InF_3[59]	2.2	4-45	~30	Resistivity = $2*10^5$ Ω·m at room temperature
CuBr[183]	2.92	0.9-8.8	~45	High photo response (3.17 A/W), high EQE (1126%)
Ta_2O_5[88]	3.8-5.3	1-30	~30	k = 15.5, SS = 61-64 mV/dec (MoS_2)
HfO_2[89,176]	~5.5	5-10	~20	k ~ 15, E_b = 0.5-0.6 V/nm. SS = 100 mV/dec (MoS_2), 67 mV/dec (HfS_2)
$SrTiO_3$[93]	3.2	5-30	Wafer scale	k = 30-100, SS = 71.5 mV/dec (MoS_2)
ITO[97]	3.9	~1.5	Wafer scale	R_S = 5.4 kΩ/sq, Transmittance = 99.3%
MoP[57]	N/A	3-10	~30	Edge-plane similar HER performance
Mo_5N_6[86]	N/A	2-40	~20	High electrical conductivity (229.6 S/cm)
δ-MoN[86]	N/A	2-40	~20	High electrical conductivity (3126 S/cm)
Mo_2C[135]	N/A	6-60	~20	R_S = 123.6 Ω/sq, $n(e)_{2D}$ = $5.84*10^{13}$ cm^{-2}
W_5N_6[184]	N/A	1.4	Wafer scale	R_S ~ 20 kΩ/sq, mobility = 35.4 $cm^2 \cdot V^{-1} \cdot s^{-1}$

Note: T_N = Neel temperature, EQE = external quantum efficiency, k = dielectric constant, SS = subthreshold swing, R_S = sheet resistance, HER = hydrogen evolution reaction, $n(e)_{2D}$ = two-dimensional electron concentration

References

(1) K. S. Novoselov et al. Electric Field Effect in Atomically Thin Carbon Films. *Science.* **2004**, *306*, 666–669.

(2) Das, S.; Robinson, J. A.; Dubey, M.; Terrones, H.; Terrones, M. Beyond Graphene: Progress in Novel Two-Dimensional Materials and van Der Waals Solids. *Annu. Rev. Mater. Res.* **2015**, *45*, 1–27.

(3) Liu, Y.; Weiss, N. O.; Duan, X.; Cheng, H. C.; Huang, Y.; Duan, X. Van Der Waals Heterostructures and Devices. *Nat. Rev. Mater.* **2016**, *1*.

(4) Novoselov, K. S.; Mishchenko, A.; Carvalho, A.; Castro Neto, A. H. 2D Materials and van Der Waals Heterostructures. *Science.* **2016**, *353*, aac9439.

(5) Rai, A.; Movva, H. C. P.; Roy, A.; Taneja, D.; Chowdhury, S.; Banerjee, S. K. Progress in Contact, Doping and Mobility Engineering of MoS_2: An Atomically Thin 2D Semiconductor. *Crystals* **2018**; *8*, 316.

(6) Naguib, M.; Mochalin, V. N.; Barsoum, M. W.; Gogotsi, Y. 25th Anniversary Article: MXenes: A New Family of Two-Dimensional Materials. *Adv. Mater.* **2014**, *26*, 992–1005.

(7) Kharadi, M. A.; Malik, G. F. A.; Khanday, F. A.; Shah, K. A.; Mittal, S.; Kaushik, B. K. Review—Silicene: From Material to Device Applications. *ECS J. Solid State Sci. Technol.* **2020**, *9*, 115031.

(8) Allen, M. J.; Tung, V. C.; Kaner, R. B. Honeycomb Carbon: A Review of Graphene. *Chem. Rev.* **2010**, *110*, 132–145.

(9) Molaei, M. J.; Younas, M.; Rezakazemi, M. A Comprehensive Review on Recent Advances in Two-Dimensional (2D) Hexagonal Boron Nitride. *ACS Appl. Electron. Mater.* **2021**, *3*, 5165–5187.

(10) Balan, A. P.; Puthirath, A. B.; Roy, S.; Costin, G.; Oliveira, E. F.; Saadi, M. A. S. R.; Sreepal, V.; Friedrich, R.; Serles, P.; Biswas, A.; Iyengar, S. A.; Chakingal, N.; Bhattacharyya, S.; Saju, S. K.; Pardo, S. C.; Sassi, L. M.; Filleter, T.; Krasheninnikov, A.; Galvao, D. S.; Vajtai, R.; Nair, R. R.; Ajayan, P. M. Non-van Der Waals Quasi-2D Materials; Recent Advances in Synthesis, Emergent Properties and Applications. *Mater. Today* **2022**, *58*, 164–200.

(11) Jin, C.; Kou, L. Two-Dimensional Non-van Der Waals Magnetic Layers: Functional Materials for Potential Device Applications. *J. Phys. D. Appl. Phys.* **2021**, *54*, 413001.

(12) Ren, S.; Tan, Q.; Zhang, J. Review on the Quantum Emitters in Two-Dimensional Materials. *J. Semicond.* **2019**, *40*, 071903.

(13) Yu, Y.; Zhang, K.; Parks, H.; Babar, M.; Carr, S.; Craig, I. M.; Van Winkle, M.; Lyssenko, A.; Taniguchi, T.; Watanabe, K.; Viswanathan, V.; Bediako, D. K. Tunable Angle-Dependent Electrochemistry at Twisted Bilayer Graphene with Moiré Flat Bands. *Nat. Chem.* **2022**, *14*, 267–273.

(14) Samy, O.; Zeng, S.; Birowosuto, M. D.; El Moutaouakil, A. A Review on MoS_2

Properties, Synthesis, Sensing Applications and Challenges. *Crystals* **2021**, *11*, 1–24.

(15) Kumar, V. P.; Panda, D. K. Review—Next Generation 2D Material Molybdenum Disulfide (MoS_2): Properties, Applications and Challenges. *ECS J. Solid State Sci. Technol.* **2022**, *11*, 033012.

(16) Koperski, M.; Nogajewski, K.; Arora, A.; Cherkez, V.; Mallet, P.; Veuillen, J. Y.; Marcus, J.; Kossacki, P.; Potemski, M. Single Photon Emitters in Exfoliated WSe_2 Structures. *Nat. Nanotechnol.* **2015**, *10*, 503–506.

(17) Tran, T. T.; Elbadawi, C.; Totonjian, D.; Lobo, C. J.; Grosso, G.; Moon, H.; Englund, D. R.; Ford, M. J.; Aharonovich, I.; Toth, M. Robust Multicolor Single Photon Emission from Point Defects in Hexagonal Boron Nitride. *ACS Nano.* **2017**, *10*, 7331–7338.

(18) Mak, K. F.; Lee, C.; Hone, J.; Shan, J.; Heinz, T. F. Atomically Thin MoS_2: A New Direct-Gap Semiconductor. *Phys. Rev. Lett.* **2010**, *105*, 136805 .

(19) Jiang, J.; Chen, Z.; Hu, Y.; Xiang, Y.; Zhang, L.; Wang, Y.; Wang, G. C.; Shi, J. Flexo-Photovoltaic Effect in MoS_2. *Nat. Nanotechnol.* **2021**, *16*, 894-901.

(20) Roy, T.; Tosun, M.; Kang, J. S.; Sachid, A. B.; Desai, S. B.; Hettick, M.; Hu, C. C.; Javey, A. Field-Effect Transistors Built from All Two-Dimensional Material Components. *ACS Nano* **2014**, *8*, 6259–6264.

(21) Zhang, X.; Grajal, J.; Vazquez-Roy, J. L.; Radhakrishna, U.; Wang, X.; Chern, W.; Zhou, L.; Lin, Y.; Shen, P. C.; Ji, X.; Ling, X.; Zubair, A.; Zhang, Y.; Wang, H.; Dubey, M.; Kong, J.; Dresselhaus, M.; Palacios, T. Two-Dimensional MoS_2-Enabled Flexible Rectenna for Wi-Fi-Band Wireless Energy Harvesting. *Nature* **2019**, *566*, 368–372.

(22) Radisavljevic, B.; Kis, A. Mobility Engineering and a Metal-Insulator Transition in Monolayer MoS_2. *Nat. Mater.* **2013**, *12*, 815–820.

(23) Radisavljevic, B.; Radenovic, A.; Brivio, J.; Giacometti, V.; Kis, A. Single-Layer MoS_2 Transistors. *Nat. Nanotechnol.* **2011**, *6*, 147–150.

(24) Zhai, Y.; Yang, X.; Wang, F.; Li, Z.; Ding, G.; Qiu, Z.; Wang, Y.; Zhou, Y.; Han, S. T. Infrared-Sensitive Memory Based on Direct-Grown MoS_2–Upconversion-Nanoparticle Heterostructure. *Adv. Mater.* **2018**, *30*, 1803563.

(25) Grosso, G.; Moon, H.; Lienhard, B.; Ali, S.; Efetov, D. K.; Furchi, M. M.; Jarillo-Herrero, P.; Ford, M. J.; Aharonovich, I.; Englund, D. Tunable and High-Purity Room Temperature Single-Photon Emission from Atomic Defects in Hexagonal Boron Nitride. *Nat. Commun.* **2017**, *8*, 1–8.

(26) Kern, J.; Niehues, I.; Tonndorf, P.; Schmidt, R.; Wigger, D.; Schneider, R.; Stiehm, T.; Michaelis de Vasconcellos, S.; Reiter, D. E.; Kuhn, T.; Bratschitsch, R. Nanoscale Positioning of Single-Photon Emitters in Atomically Thin WSe_2. *Adv. Mater.* **2016**, *28*, 7101–7105.

(27) Li, R.; Ma, X.; Li, J.; Cao, J.; Gao, H.; Li, T.; Zhang, X.; Wang, L.; Zhang, Q.; Wang, G.; Hou, C.; Li, Y.; Palacios, T.; Lin, Y.; Wang, H.; Ling, X. Flexible and High-Performance Electrochromic Devices Enabled by Self-Assembled 2D TiO_2/MXene Heterostructures.

Nat. Commun. **2021**, *12*, 1–11.

(28) Bae, S.; Kim, H.; Lee, Y.; Xu, X.; Park, J. S.; Zheng, Y.; Balakrishnan, J.; Lei, T.; Ri Kim, H.; Song, Y. Il; Kim, Y. J.; Kim, K. S.; Özyilmaz, B.; Ahn, J. H.; Hong, B. H.; Iijima, S. Roll-to-Roll Production of 30-Inch Graphene Films for Transparent Electrodes. *Nat. Nanotechnol.* **2010**, *5*, 574–578.

(29) Sun, Z.; Martinez, A.; Wang, F. Optical Modulators with 2D Layered Materials. *Nat. Photonics* **2016**, *10*, 227–238.

(30) Tran, K.; Choi, J.; Singh, A. Moiré and beyond in Transition Metal Dichalcogenide Twisted Bilayers. *2D Mater.* **2021**, *8*, 022002.

(31) Nimbalkar, A.; Kim, H. Opportunities and Challenges in Twisted Bilayer Graphene: A Review. *Nano-Micro Lett.* **2020**, *12*, 1–20.

(32) Lin, X.; Yang, W.; Wang, K. L.; Zhao, W. Two-Dimensional Spintronics for Low-Power Electronics. *Nat. Electron.* **2019**, *2*, 274–283.

(33) Liu, B.; Abbas, A.; Zhou, C. Two-Dimensional Semiconductors: From Materials Preparation to Electronic Applications. *Adv. Electron. Mater.* **2017**, *3*, 1–17.

(34) Naumis, G. G.; Barraza-Lopez, S.; Oliva-Leyva, M.; Terrones, H. Electronic and Optical Properties of Strained Graphene and Other Strained 2D Materials: A Review. *Reports Prog. Phys.* **2017**, *80*, 096501.

(35) Gibertini, M.; Koperski, M.; Morpurgo, A. F.; Novoselov, K. S. Magnetic 2D Materials and Heterostructures. *Nat. Nanotechnol.* **2019**, *14*, 408–419.

(36) Lozovoy, K. A.; Korotaev, A. G.; Kokhanenko, A. P.; Dirko, V. V.; Voitsekhovskii, A. V. Kinetics of Epitaxial Formation of Nanostructures by Frank–van Der Merwe, Volmer–Weber and Stranski–Krastanow Growth Modes. *Surf. Coatings Technol.* **2020**, *384*, 125289.

(37) Joyce, B. A.; Vvedensky, D. D.; Bell, G. R.; Belk, J. G.; Itoh, M.; Jones, T. S. Nucleation and Growth Mechanisms during MBE of III-V Compounds. *Mater. Sci. Eng. B Solid-State Mater. Adv. Technol.* **1999**, *67*, 7–16.

(38) Joyce, B. A.; Vvedensky, D. D.; Avery, A. R.; Belk, J. G.; Dobbs, H. T.; Jones, T. S. Nucleation Mechanisms during MBE Growth of Lattice-Matched and Strained III-V Compound Films. *Appl. Surf. Sci.* **1998**, *130*, 357–366.

(39) Daudin, B.; Widmann, F.; Feuillet, G.; Samson, Y.; Arlery, M.; Rouvière, J. Stranski-Krastanov Growth Mode during the Molecular Beam Epitaxy of Highly Strained GaN. *Phys. Rev. B* **1997**, *56*, R7069.

(40) Foadi, F.; Ten Brink, G. H.; Mohammadizadeh, M. R.; Palasantzas, G. Roughness Dependent Wettability of Sputtered Copper Thin Films: The Effect of the Local Surface Slope. *J. Appl. Phys.* **2019**, *125*, 244307.

(41) Schmiedl, E.; Wissmann, P.; Finzel, H. U. The Electrical Resistivity of Ultra-Thin Copper Films. *Zeitschrift fur Naturforsch. A.* **2008**, *63*, 739–744.

(42) Lee, Y. S.; Shim, T. H.; Yoo, S. D.; Park, J. G. Silicon Thickness Fluctuation Scattering Dependence of Electron Mobility in Ultrathin Body Silicon-on-Insulator n -Metal-Oxide-Semiconductor Field-Effect Transistors. *J. Appl. Phys.* **2008**, *103*, 084503.

(43) Morkoç, H. III-Nitride Semiconductor Growth by MBE: Recent Issues. *J. Mater. Sci. Mater. Electron.* **2001**, *12*, 677–695.

(44) Wang, L.; Meric, I.; Huang, P. Y.; Gao, Q.; Gao, Y.; Tran, H.; Taniguchi, T.; Watanabe, K.; Campos, L. M.; Muller, D. A.; Guo, J.; Kim, P.; Hone, J.; Shepard, K. L.; Dean, C. R. One-Dimensional Electrical Contact to a Two-Dimensional Material. *Science.* **2013**, *342*, 614–617.

(45) Splendiani, A.; Sun, L.; Zhang, Y.; Li, T.; Kim, J.; Chim, C. Y.; Galli, G.; Wang, F. Emerging Photoluminescence in Monolayer MoS_2. *Nano Lett.* **2010**, *10*, 1271–1275.

(46) Riedl, C.; Coletti, C.; Starke, U. Structural and Electronic Properties of Epitaxial Graphene on SiC(0001): A Review of Growth, Characterization, Transfer Doping and Hydrogen Intercalation. *J. Phys. D. Appl. Phys.* **2010**, *43*, 374009.

(47) Raza, H. Graphene Nanoelectronics: Metrology, Synthesis, Properties, and Applications. *Springer Science & Business Media* **2012**; Vol. 6.

(48) Tu, H. W.; Shih, C. C.; Lin, C. L.; Yu, M. Z.; Lai, J. J.; Luo, J. C.; Lin, G. L.; Jian, W. Bin; Watanabe, K.; Taniguchi, T.; Hu, C. High Field-Effect Performance and Intrinsic Scattering in the Two-Dimensional MoS_2 Semiconductors. *Appl. Surf. Sci.* **2021**, *564*, 150422.

(49) Shen, T.; Li, F.; Xu, L.; Zhang, Z.; Qiu, F.; Li, Z.; Qi, J. High Mobility Monolayer MoS_2 Transistors and Its Charge Transport Behaviour under E-Beam Irradiation. *J. Mater. Sci.* **2020**, *55*, 14315–14325.

(50) Huo, N.; Yang, Y.; Wu, Y. N.; Zhang, X. G.; Pantelides, S. T.; Konstantatos, G. High Carrier Mobility in Monolayer CVD-Grown MoS_2 through Phonon Suppression. *Nanoscale* **2018**, *10*, 15071–15077.

(51) Kim, C.; Moon, I.; Lee, D.; Choi, M. S.; Ahmed, F.; Nam, S.; Cho, Y.; Shin, H. J.; Park, S.; Yoo, W. J. Fermi Level Pinning at Electrical Metal Contacts of Monolayer Molybdenum Dichalcogenides. *ACS Nano* **2017**, *11*, 1588–1596.

(52) Liu, X.; Choi, M. S.; Hwang, E.; Yoo, W. J.; Sun, J. Fermi Level Pinning Dependent 2D Semiconductor Devices: Challenges and Prospects. *Adv. Mater.* **2022**, *34*, 2108425.

(53) Cheon, G.; Duerloo, K. A. N.; Sendek, A. D.; Porter, C.; Chen, Y.; Reed, E. J. Data Mining for New Two- and One-Dimensional Weakly Bonded Solids and Lattice-Commensurate Heterostructures. *Nano Lett.* **2017**, *17*, 1915–1923.

(54) Takahashi, K., Yoshikawa, A., & Sandhu, A. Wide Bandgap Semiconductors. *Verlag Berlin Heidelberg* **2007**.

(55) Yang, Y. J.; Ho, W. S.; Huang, C. F.; Chang, S. T.; Liu, C. W. Electron Mobility Enhancement in Strained-Germanium n -Channel Metal-Oxide-Semiconductor Field-Effect Transistors. *Appl. Phys. Lett.* **2007**, *91* (10). https://doi.org/10.1063/1.2779845.

(56) Robertson, J. High Dielectric Constant Oxides. *Eur. Phys. JournalApplied Phys.* **2006**, *184*, 177–184.

(57) Zhang, C.; Lu, W.; Xu, Y.; Zeng, K.; Ho, G. W. Mechanistic Formulation of Inorganic Membranes at the Air–Liquid Interface. *Nature* **2023**, *616*, 293-299.

(58) Frisenda, R.; Niu, Y.; Gant, P.; Muñoz, M.; Castellanos-Gomez, A. Naturally Occurring van Der Waals Materials. *npj 2D Materials and Applications*. **2020**, *4*, 1–13.

(59) Li, Y.; Li, Y. L.; Sa, B.; Ahuja, R. Review of Two-Dimensional Materials for Photocatalytic Water Splitting from a Theoretical Perspective. *Catalysis Science and Technology*. **2017**, *7*, 545–559.

(60) Yang, X.; Singh, D.; Ahuja, R. Recent Advancements and Future Prospects in Ultrathin 2d Semiconductor-Based Photocatalysts for Water Splitting. *Catalysts* **2020**, *10*, 1–50.

(61) Li, T.; Luo, W.; Kitadai, H.; Wang, X.; Ling, X. Probing the Domain Architecture in 2D α-Mo_2C via Polarized Raman Spectroscopy. *Adv. Mater.* **2019**, *31*, 1–9.

(62) Cao, J.; Li, T.; Gao, H.; Lin, Y.; Wang, X.; Wang, H.; Palacios, T.; Ling, X. Realization of 2D Crystalline Metal Nitrides via Selective Atomic Substitution. *Sci. Adv.* **2020**, *6*, eaax8784.

(63) Cao, J.; Li, T.; Gao, H.; Cong, X.; Lin, M. L.; Russo, N.; Luo, W.; Ding, S.; Wang, Z.; Smith, K. E.; Tan, P. H.; Ma, Q.; Ling, X. Ultrathin GaN Crystal Realized Through Nitrogen Substitution of Layered GaS. *J. Electron. Mater.* **2023**, *52*, 7551-7565.

(64) Si, J.; Yu, J.; Lan, H.; Niu, L.; Luo, J.; Yu, Y.; Li, L.; Ding, Y.; Zeng, M.; Fu, L. Chemical Potential-Modulated Ultrahigh-Phase-Purity Growth of Ultrathin Transition-Metal Boride Single Crystals. *J. Am. Chem. Soc.* **2022** *145*, 3994-4002.

(65) Wang, W.; Qi, J.; Zhai, L.; Ma, C.; Ke, C.; Zhai, W.; Wu, Z.; Bao, K.; Yao, Y.; Li, S.; Chen, B.; Repaka, D. V. M.; Zhang, X.; Ye, R.; Lai, Z.; Luo, G.; Chen, Y.; He, Q. Preparation of 2D Molybdenum Phosphide via Surface-Confined Atomic Substitution. *Adv. Mater.* **2022**, *34*, 1–11.

(66) Zhao, M.; Yang, S.; Zhang, K.; Zhang, L.; Chen, P.; Yang, S.; Zhao, Y.; Ding, X.; Zu, X.; Li, Y.; Zhao, Y.; Qiao, L.; Zhai, T. A Universal Atomic Substitution Conversion Strategy Towards Synthesis of Large-Size Ultrathin Nonlayered Two-Dimensional Materials. *Nano-Micro Lett.* **2021**, *13*, 1–13.

(67) Sreepal, V.; Yagmurcukardes, M.; Vasu, K. S.; Kelly, D. J.; Taylor, S. F. R.; Kravets, V. G.; Kudrynskyi, Z.; Kovalyuk, Z. D.; Patanè, A.; Grigorenko, A. N.; Haigh, S. J.; Hardacre, C.; Eaves, L.; Sahin, H.; Geim, A. K.; Peeters, F. M.; Nair, R. R. Two-Dimensional Covalent Crystals by Chemical Conversion of Thin van Der Waals Materials. *Nano Lett.* **2019**, *19*, 6475–6481.

(68) Hu, X.; Huang, P.; Liu, K.; Jin, B.; Zhang, X.; Zhang, X.; Zhou, X.; Zhai, T. Salt-Assisted Growth of Ultrathin GeSe Rectangular Flakes for Phototransistors with Ultrahigh Responsivity. *ACS Appl. Mater. Interfaces* **2019**, *11*, 23353-23360.

(69) Zavabeti, A.; Ou, J. Z.; Carey, B. J.; Syed, N.; Orrell-Trigg, R.; Mayes, E. L. H.; Xu, C.;

Kavehei, O.; O'Mullane, A. P.; Kaner, R. B.; Kalantar-Zadeh, K.; Daeneke, T. A Liquid Metal Reaction Environment for the Room-Temperature Synthesis of Atomically Thin Metal Oxides. *Science.* **2017**, *358*, 332–335.

(70) Samal, R.; Sanyal, G.; Chakraborty, B.; Rout, C. S. Two-Dimensional Transition Metal Phosphorous Trichalcogenides (MPX_3): A Review on Emerging Trends, Current State and Future Perspectives. *J. Mater. Chem. A* **2021**, *9*, 2560–2591.

(71) Du, L.; Huang, Y.; Wang, Y.; Wang, Q.; Yang, R.; Tang, J.; Liao, M.; Shi, D.; Shi, Y.; Zhou, X.; Zhang, Q.; Zhang, G. 2D Proximate Quantum Spin Liquid State in Atomic-Thin α-$RuCl_3$. *2D Mater.* **2019**, *6*, 015014.

(72) Fu, Y.; He, D.; He, J.; Han, X.; Bai, J.; Wang, Y.; Zhao, H. Photocarrier Dynamics in TlGaS2Nanoflakes and van Der Waals Heterostructures with Hexagonal Boron Nitride and WS_2 Nanoflakes: Implications for Optoelectronic Applications. *ACS Appl. Nano Mater.* **2020**, *3*, 8702–8707.

(73) Zhang, L.; Kang, W.; Ma, Q.; Xie, Y.; Jia, Y.; Deng, N.; Zhang, Y.; Ju, J.; Cheng, B. Two-Dimensional Acetate-Based Light Lanthanide Fluoride Nanomaterials (F-Ln, Ln = La, Ce, Pr, and Nd): Morphology, Structure, Growth Mechanism, and Stability. *J. Am. Chem. Soc.* **2019**, *141*, 13134–13142.

(74) Jiang, S.; Shan, J.; Mak, K. F. Electric-Field Switching of Two-Dimensional van Der Waals Magnets. *Nat. Mater.* **2018**, *17*, 406–410.

(75) Ci, X.; Zhao, W.; Luo, J.; Wu, Y.; Ge, T.; Shen, L.; Gao, X.; Fang, Z. Revealing the Lubrication Mechanism of Fluorographene Nanosheets Enhanced GTL-8 Based Nanolubricant Oil. *Tribol. Int.* **2019**, *138*, 174–183.

(76) Liu, J.; Xue, Y.; Wang, Z.; Xu, Z. Q.; Zheng, C.; Weber, B.; Song, J.; Wang, Y.; Lu, Y.; Zhang, Y.; Bao, Q. Two-Dimensional $CH_3NH_3PbI_3$ Perovskite: Synthesis and Optoelectronic Application. *ACS Nano* **2016**, *10*, 3536–3542.

(77) Suslu, A.; Wu, K.; Sahin, H.; Chen, B.; Yang, S.; Cai, H.; Aoki, T.; Horzum, S.; Kang, J.; Peeters, F. M.; Tongay, S. Unusual Dimensionality Effects and Surface Charge Density in 2D $Mg(OH)_2$. *Sci. Rep.* **2016**, *6*, 1–7.

(78) Aykol, M.; Kim, S.; Wolverton, C. Van Der Waals Interactions in Layered Lithium Cobalt Oxides. *J. Phys. Chem. C* **2015**, *119*, 19053–19058.

(79) Gao, X.; Zhang, H.; Guo, E.; Yao, F.; Wang, Z.; Yue, H. Hybrid Two-Dimensional Nickel Oxide-Reduced Graphene Oxide Nanosheets for Supercapacitor Electrodes. *Microchem. J.* **2021**, *164*, 105979.

(80) Luo, S.; Zhu, X.; Liu, H.; Song, S.; Chen, Y.; Liu, C.; Zhou, W.; Tang, C.; Shao, G.; Jin, Y.; Guan, J.; Tung, V. C.; Li, H.; Chen, X.; Ouyang, F.; Liu, S. Direct Growth of Magnetic Non-van Der Waals Cr_2X_3 (X = S, Se, and Te) on SiO2/Si Substrates through the Promotion of KOH. *Chem. Mater.* **2022**, *34*, 2342–2351.

(81) Mounet, N.; Gibertini, M.; Schwaller, P.; Campi, D.; Merkys, A.; Marrazzo, A.; Sohier, T.; Castelli, I. E.; Cepellotti, A.; Pizzi, G.; Marzari, N. Two-Dimensional Materials from High-Throughput Computational Exfoliation of Experimentally Known Compounds. *Nat.*

Nanotechnol. **2018**, *13*, 246–252.

(82) Wagner, S. 2D Materials for Piezoresistive Strain Gauges and Membrane Based Nanoelectromechanical Systems. *Dr. Diss. RWTH Aachen Univ.* **2018**, 1–168.

(83) Huang, J.-K.; Wan, Y.; Shi, J.; Zhang, J.; Wang, Z.; Wang, W.; Yang, N.; Liu, Y.; Lin, C.-H.; Guan, X.; Hu, L.; Yang, Z.-L.; Huang, B.-C.; Chiu, Y.-P.; Yang, J.; Tung, V.; Wang, D.; Kalantar-Zadeh, K.; Wu, T.; Zu, X.; Qiao, L.; Li, L.-J.; Li, S. High-κ Perovskite Membranes as Insulators for Two-Dimensional Transistors. *Nature* **2022**, *605*, 262–267.

(84) Hu, X.; Huang, P.; Jin, B.; Zhang, X.; Li, H.; Zhou, X.; Zhai, T. Halide-Induced Self-Limited Growth of Ultrathin Nonlayered Ge Flakes for High-Performance Phototransistors. *J. Am. Chem. Soc.* **2018**, *140*, 12909–12914.

(85) Chu, J.; Zhang, Y.; Wen, Y.; Qiao, R.; Wu, C.; He, P.; Yin, L.; Cheng, R.; Wang, F.; Wang, Z.; Xiong, J.; Li, Y.; He, J. Sub-Millimeter-Scale Growth of One-Unit-Cell-Thick Ferrimagnetic Cr_2S_3 Nanosheets. *Nano Lett.* **2019**, *19*, 2154–2161.

(86) Yin, C.; Gong, C.; Chu, J.; Wang, X.; Yan, C.; Qian, S.; Wang, Y.; Rao, G.; Wang, H.; Liu, Y.; Wang, X.; Wang, J.; Hu, W.; Li, C.; Xiong, J. Ultrabroadband Photodetectors up to 10.6 μm Based on 2D Fe_3O_4 Nanosheets. *Adv. Mater.* **2020**, *32*, 4–11.

(87) Datta, R. S.; Syed, N.; Zavabeti, A.; Jannat, A.; Mohiuddin, M.; Rokunuzzaman, M.; Yue Zhang, B.; Rahman, M. A.; Atkin, P.; Messalea, K. A.; Ghasemian, M. B.; Gaspera, E. Della; Bhattacharyya, S.; Fuhrer, M. S.; Russo, S. P.; McConville, C. F.; Esrafilzadeh, D.; Kalantar-Zadeh, K.; Daeneke, T. Flexible Two-Dimensional Indium Tin Oxide Fabricated Using a Liquid Metal Printing Technique. *Nat. Electron.* **2020**, *3*, 51–58.

(88) Jin, T.; Zheng, Y.; Gao, J.; Wang, Y.; Li, E.; Chen, H.; Pan, X.; Lin, M.; Chen, W. Controlling Native Oxidation of HfS_2 for 2D Materials Based Flash Memory and Artificial Synapse. *ACS Appl. Mater. Interfaces* **2021**, *13*, 10639–10649.

(89) Chahal, S.; Kauzlarich, S. M.; Kumar, P. Microwave Synthesis of Hematene and Other Two-Dimensional Oxides. *ACS Mater. Lett.* **2021**, *3*, 631–640.

(90) Xu, C.; Wang, L.; Liu, Z.; Chen, L.; Guo, J.; Kang, N.; Ma, X. L.; Cheng, H. M.; Ren, W. Large-Area High-Quality 2D Ultrathin Mo_2C Superconducting Crystals. *Nat. Mater.* **2015**, *14*, 1135–1141.

(91) Gao, H.; Cao, J.; Li, T.; Luo, W.; Gray, M.; Kumar, N.; Burch, K. S.; Ling, X. Phase-Controllable Synthesis of Ultrathin Molybdenum Nitride Crystals Via Atomic Substitution of MoS_2. *Chem. Mater.* **2022**, *34*, 351–357.

(92) Cui, Q.; Sakhdari, M.; Chamlagain, B.; Chuang, H. J.; Liu, Y.; Cheng, M. M. C.; Zhou, Z.; Chen, P. Y. Ultrathin and Atomically Flat Transition-Metal Oxide: Promising Building Blocks for Metal-Insulator Electronics. *ACS Appl. Mater. Interfaces* **2016**, *8*, 34552–34558.

(93) Chamlagain, B.; Cui, Q.; Paudel, S.; Cheng, M. M. C.; Chen, P. Y.; Zhou, Z. Thermally Oxidized 2D TaS2 as a High-κ Gate Dielectric for MoS_2 Field-Effect Transistors. *2D Mater.* **2017**, *4*, 031002.

(94) Lai, S.; Byeon, S.; Jang, S. K.; Lee, J.; Lee, B. H.; Park, J. H.; Kim, Y. H.; Lee, S. HfO_2/HfS_2 Hybrid Heterostructure Fabricated: Via Controllable Chemical Conversion of Two-Dimensional HfS_2. *Nanoscale* **2018**, *10*, 18758–18766.

(95) Chen, Y.; Liu, K.; Liu, J.; Lv, T.; Wei, B.; Zhang, T.; Zeng, M.; Wang, Z.; Fu, L. Growth of 2D GaN Single Crystals on Liquid Metals. *J. Am. Chem. Soc.* **2018**, *140*, 16392–16395.

(96) Lee, M. J.; Ahn, J. H.; Sung, J. H.; Heo, H.; Jeon, S. G.; Lee, W.; Song, J. Y.; Hong, K. H.; Choi, B.; Lee, S. H.; Jo, M. H. Thermoelectric Materials by Using Two-Dimensional Materials with Negative Correlation between Electrical and Thermal Conductivity. *Nat. Commun.* **2016**, *7*, 1–7.

(97) Peimyoo, N.; Barnes, M. D.; Mehew, J. D.; De Sanctis, A.; Amit, I.; Escolar, J.; Anastasiou, K.; Rooney, A. P.; Haigh, S. J.; Russo, S.; Craciun, M. F.; Withers, F. Laser-Writable High-k Dielectric for van Der Waals Nanoelectronics. *Sci. Adv.* **2019**, *5*, eaau0906.

(98) Ling, X.; Lee, Y. H.; Lin, Y.; Fang, W.; Yu, L.; Dresselhaus, M. S.; Kong, J. Role of the Seeding Promoter in MoS_2 Growth by Chemical Vapor Deposition. *Nano Lett.* **2014**, *14*, 464–472.

(99) Velický, M.; Donnelly, G. E.; Hendren, W. R.; McFarland, S.; Scullion, D.; DeBenedetti, W. J. I.; Correa, G. C.; Han, Y.; Wain, A. J.; Hines, M. A.; Muller, D. A.; Novoselov, K. S.; Abruña, H. D.; Bowman, R. M.; Santos, E. J. G.; Huang, F. Mechanism of Gold-Assisted Exfoliation of Centimeter-Sized Transition-Metal Dichalcogenide Monolayers. *ACS Nano* **2018**, *12*, 10463–10472.

(100) Huang, Y.; Pan, Y. H.; Yang, R.; Bao, L. H.; Meng, L.; Luo, H. L.; Cai, Y. Q.; Liu, G. D.; Zhao, W. J.; Zhou, Z.; Wu, L. M.; Zhu, Z. L.; Huang, M.; Liu, L. W.; Liu, L.; Cheng, P.; Wu, K. H.; Tian, S. B.; Gu, C. Z.; Shi, Y. G.; Guo, Y. F.; Cheng, Z. G.; Hu, J. P.; Zhao, L.; Yang, G. H.; Sutter, E.; Sutter, P.; Wang, Y. L.; Ji, W.; Zhou, X. J.; Gao, H. J. Universal Mechanical Exfoliation of Large-Area 2D Crystals. *Nat. Commun.* **2020**, *11*, 2453.

(101) Zhu, J.; Park, J. H.; Vitale, S. A.; Ge, W.; Jung, G. S.; Wang, J.; Mohamed, M.; Zhang, T.; Ashok, M.; Xue, M.; Zheng, X.; Wang, Z.; Hansryd, J.; Chandrakasan, A. P.; Kong, J.; Palacios, T. Low-Thermal-Budget Synthesis of Monolayer Molybdenum Disulfide for Silicon Back-End-of-Line Integration on a 200 Mm Platform. *Nat. Nanotechnol.* **2023**, *18*, 456–463.

(102) Li, T.; Guo, W.; Ma, L.; Li, W.; Yu, Z.; Han, Z.; Gao, S.; Liu, L.; Fan, D.; Wang, Z.; Yang, Y.; Lin, W.; Luo, Z.; Chen, X.; Dai, N.; Tu, X.; Pan, D.; Yao, Y.; Wang, P.; Nie, Y.; Wang, J.; Shi, Y.; Wang, X. Epitaxial Growth of Wafer-Scale Molybdenum Disulfide Semiconductor Single Crystals on Sapphire. *Nat. Nanotechnol.* **2021**, *16*, 1201–1207.

(103) Zheng, W.; Lee, L. Y. S. Beyond Sonication: Advanced Exfoliation Methods for Scalable Production of 2D Materials. *Matter* **2022**, *5*, 515–545.

(104) Liu, F.; Wu, W.; Bai, Y.; Chae, S. H.; Li, Q.; Wang, J.; Hone, J.; Zhu, X. Y. Disassembling 2D van Der Waals Crystals into Macroscopic Monolayers and Reassembling into Artificial Lattices. *Science.* **2020**, *367*, 903–906.

(105) Lam, D.; Lebedev, D.; Hersam, M. C. Morphotaxy of Layered van Der Waals Materials. *ACS Nano* **2022**, *16*, 7144–7167.

(106) Tantis, I.; Talande, S.; Tzitzios, V.; Basina, G.; Shrivastav, V.; Bakandritsos, A.; Zboril, R. Non-van Der Waals 2D Materials for Electrochemical Energy Storage. *Adv. Funct. Mater.* **2023**, *33*, 2209360.

(107) Xu, Y.; Cao, H.; Xue, Y.; Li, B.; Cai, W. Liquid-Phase Exfoliation of Graphene: An Overview on Exfoliation Media, Techniques, and Challenges. *Nanomaterials* **2018**, *8*, 942.

(108) Naguib, M.; Kurtoglu, M.; Presser, V.; Lu, J.; Niu, J.; Heon, M.; Hultman, L.; Gogotsi, Y.; Barsoum, M. W. Two-Dimensional Nanocrystals Produced by Exfoliation of Ti_3AlC_2. *Adv. Mater.* **2011**, *23*, 4248–4253.

(109) Jiang, S.; Arguilla, M. Q.; Cultrara, N. D.; Goldberger, J. E. Covalently-Controlled Properties by Design in Group IV Graphane Analogues. *Acc. Chem. Res.* **2015**, *48*, 144–151.

(110) Anasori, B.; Lukatskaya, M. R.; Gogotsi, Y. 2D Metal Carbides and Nitrides (MXenes) for Energy Storage. *Nat. Rev. Mater.* **2017**, *2*, 1-17.

(111) Anasori, B.; Gogotsi, Y. 2D Metal Carbides and Nitrides (MXenes): Structure, Properties and Applications; *Springer Nature Switzerland AG* **2019**.

(112) Hong Ng, V. M.; Huang, H.; Zhou, K.; Lee, P. S.; Que, W.; Xu, J. Z.; Kong, L. B. Recent Progress in Layered Transition Metal Carbides and/or Nitrides (MXenes) and Their Composites: Synthesis and Applications. *J. Mater. Chem. A* **2017**, *5*, 3039–3068.

(113) Anasori, B.; Xie, Y.; Beidaghi, M.; Lu, J.; Hosler, B. C.; Hultman, L.; Kent, P. R. C.; Gogotsi, Y.; Barsoum, M. W. Two-Dimensional, Ordered, Double Transition Metals Carbides (MXenes). *ACS Nano* **2015**, *9*, 9507–9516.

(114) Puthirath Balan, A.; Radhakrishnan, S.; Woellner, C. F.; Sinha, S. K.; Deng, L.; Reyes, C. D. L.; Rao, B. M.; Paulose, M.; Neupane, R.; Apte, A.; Kochat, V.; Vajtai, R.; Harutyunyan, A. R.; Chu, C. W.; Costin, G.; Galvao, D. S.; Martí, A. A.; Van Aken, P. A.; Varghese, O. K.; Tiwary, C. S.; Malie Madom Ramaswamy Iyer, A.; Ajayan, P. M. Exfoliation of a Non-van Der Waals Material from Iron Ore Hematite. *Nat. Nanotechnol.* **2018**, *13*, 602–609.

(115) Xu, K.; Zhang, B. Y.; Mohiuddin, M.; Ha, N.; Wen, X.; Zhou, C.; Li, Y.; Ren, G.; Zhang, H.; Zavabeti, A.; Ou, J. Z. Free-Standing Ultra-Thin Janus Indium Oxysulfide for Ultrasensitive Visible-Light-Driven Optoelectronic Chemical Sensing. *Nano Today* **2021**, *37*, 101096.

(116) Xie, H.; Li, Z.; Cheng, L.; Haidry, A. A.; Tao, J.; Xu, Y.; Xu, K.; Ou, J. Z. Recent Advances in the Fabrication of 2D Metal Oxides. *Iscience* **2022**, *25*, 1–30.

(117) Serles, P.; Arif, T.; Puthirath, A. B.; Yadav, S.; Wang, G.; Cui, T.; Balan, A. P.; Yadav, T. P.; Thibeorchews, P.; Chakingal, N.; Costin, G.; Singh, C. V.; Ajayan, P. M.; Filleter, T. Friction of Magnetene, a Non-van Der Waals 2D Material. *Sci. Adv.* **2021**, *7*, 1–10.

(118) Liu, S.; Xie, L.; Qian, H.; Liu, G.; Zhong, H.; Zeng, H. Facile Preparation of Novel and Active 2D Nanosheets from Non-Layered and Traditionally Non-Exfoliable Earth-Abundant Materials. *J. Mater. Chem. A* **2019**, *7*, 15411–15419.

(119) Friedrich, R.; Ghorbani-Asl, M.; Curtarolo, S.; Krasheninnikov, A. V. Data-Driven Quest for Two-Dimensional Non-van Der Waals Materials. *Nano Lett.* **2022**, *22*, 989–997.

(120) Barnowsky, T.; Krasheninnikov, A. V.; Friedrich, R. A New Group of 2D Non-van Der Waals Materials with Ultra Low Exfoliation Energies. *Adv. Electron. Mater.* **2023**, *9*, 1–8.

(121) Tang, B.; Che, B.; Xu, M.; Ang, Z. P.; Di, J.; Gao, H.-J.; Yang, H.; Zhou, J.; Liu, Z. Recent Advances in Synthesis and Study of 2D Twisted Transition Metal Dichalcogenide Bilayers. *Small Struct.* **2021**, *2*, 2000153.

(122) Yu, J.; Li, J.; Zhang, W.; Chang, H. Synthesis of High Quality Two-Dimensional Materials via Chemical Vapor Deposition. *Chem. Sci.* **2015**, *6*, 6705–6716.

(123) Cai, Z.; Liu, B.; Zou, X.; Cheng, H. M. Chemical Vapor Deposition Growth and Applications of Two-Dimensional Materials and Their Heterostructures. *Chem. Rev.* **2018**, *118*, 6091–6133.

(124) Tan, C.; Chen, J.; Wu, X. J.; Zhang, H. Epitaxial Growth of Hybrid Nanostructures. *Nat. Rev. Mater.* **2018**, *3*, 1–13.

(125) Chambers, S. A. Epitaxial Growth and Properties of Thin Film Oxides. *Surf. Sci. Rep.* **2000**, *39*, 105–180.

(126) Choi, D.; Harris, J. S.; Kim, E.; McIntyre, P. C.; Cagnon, J.; Stemmer, S. High-Quality III-V Semiconductor MBE Growth on Ge/Si Virtual Substrates for Metal-Oxide-Semiconductor Device Fabrication. *J. Cryst. Growth* **2009**, *311*, 1962–1971.

(127) Al Balushi, Z. Y.; Wang, K.; Ghosh, R. K.; Vilá, R. A.; Eichfeld, S. M.; Caldwell, J. D.; Qin, X.; Lin, Y. C.; Desario, P. A.; Stone, G.; Subramanian, S.; Paul, D. F.; Wallace, R. M.; Datta, S.; Redwing, J. M.; Robinson, J. A. Two-Dimensional Gallium Nitride Realized via Graphene Encapsulation. *Nat. Mater.* **2016**, *15*, 1166–1171.

(128) Briggs, N.; Bersch, B.; Wang, Y.; Jiang, J.; Koch, R. J.; Nayir, N.; Wang, K.; Kolmer, M.; Ko, W.; De La Fuente Duran, A.; Subramanian, S.; Dong, C.; Shallenberger, J.; Fu, M.; Zou, Q.; Chuang, Y. W.; Gai, Z.; Li, A. P.; Bostwick, A.; Jozwiak, C.; Chang, C. Z.; Rotenberg, E.; Zhu, J.; van Duin, A. C. T.; Crespi, V.; Robinson, J. A. Atomically Thin Half-van Der Waals Metals Enabled by Confinement Heteroepitaxy. *Nat. Mater.* **2020**, *19*, 637–643.

(129) Zhang, W.; Naidu, B. S.; Ou, J. Z.; O'Mullane, A. P.; Chrimes, A. F.; Carey, B. J.; Wang, Y.; Tang, S. Y.; Sivan, V.; Mitchell, A.; Bhargava, S. K.; Kalantar-Zadeh, K. Liquid Metal/Metal Oxide Frameworks with Incorporated Ga_2O_3 for Photocatalysis. *ACS Appl. Mater. Interfaces* **2015**, *7*, 1943–1948.

(130) Zhang, W.; Ou, J. Z.; Tang, S. Y.; Sivan, V.; Yao, D. D.; Latham, K.; Khoshmanesh, K.; Mitchell, A.; O'Mullane, A. P.; Kalantar-Zadeh, K. Liquid Metal/Metal Oxide Frameworks. *Adv. Funct. Mater.* **2014**, *24*, 3799–3807.

(131) Syed, N.; Zavabeti, A.; Ou, J. Z.; Mohiuddin, M.; Pillai, N.; Carey, B. J.; Zhang, B. Y.; Datta, R. S.; Jannat, A.; Haque, F.; Messalea, K. A.; Xu, C.; Russo, S. P.; McConville, C. F.; Daeneke, T.; Kalantar-Zadeh, K. Printing Two-Dimensional Gallium Phosphate out of Liquid Metal. *Nat. Commun.* **2018**, *9*, 3618.

(132) Koike, J.; Hosseini, M.; Hai, H. T.; Ando, D.; Sutou, Y. Material Innovation for MOL, BEOL, and 3D Integration. *Tech. Dig. - Int. Electron Devices Meet. IEDM* **2017**, pp. 32-3.

(133) Meng, W.; Xu, F.; Yu, Z.; Tao, T.; Shao, L.; Liu, L.; Li, T.; Wen, K.; Wang, J.; He, L.; Sun, L.; Li, W.; Ning, H.; Dai, N.; Qin, F.; Tu, X.; Pan, D.; He, S.; Li, D.; Zheng, Y.; Lu, Y.; Liu, B.; Zhang, R.; Shi, Y.; Wang, X. Three-Dimensional Monolithic Micro-LED Display Driven by Atomically Thin Transistor Matrix. *Nat. Nanotechnol.* **2021**, *16*, 1231–1236.

(134) Hwangbo, S.; Hu, L.; Hoang, A. T.; Choi, J. Y.; Ahn, J. H. Wafer-Scale Monolithic Integration of Full-Colour Micro-LED Display Using MoS2 Transistor. *Nat. Nanotechnol.* **2022**, *17*, 500–506.

(135) Jeon, J.; Park, Y.; Choi, S.; Lee, J.; Lim, S. S.; Lee, B. H.; Song, Y. J.; Cho, J. H.; Jang, Y. H.; Lee, S. Epitaxial Synthesis of Molybdenum Carbide and Formation of a Mo_2C/MoS_2 Hybrid Structure via Chemical Conversion of Molybdenum Disulfide. *ACS Nano* **2018**, *12*, 338–346.

(136) Li, T.; Cao, J.; Gao, H.; Wang, Z.; Geiwitz, M.; Burch, K. S.; Ling, X. Epitaxial Atomic Substitution for MoS_2-MoN Heterostructure Synthesis. *ACS Appl. Mater. Interfaces* **2022**, *14*, 57144–57152.

(137) Li, T. 2D Non-van Der Waals Transition Metal Carbides and Nitrides : From Synthesis to Electronic Application. *Dr. Diss. Bost. Univ.* **2022**.

(138) Choi, S.; Kim, Y. J.; Jeon, J.; Lee, B. H.; Cho, J. H.; Lee, S. Scalable Two-Dimensional Lateral Metal/Semiconductor Junction Fabricated with Selective Synthetic Integration of Transition-Metal-Carbide (Mo_2C)/-Dichalcogenide (MoS_2). *ACS Appl. Mater. Interfaces* **2019**, *11*, 47190–47196.

(139) Xia, F.; Farmer, D. B.; Lin, Y. M.; Avouris, P. Graphene Field-Effect Transistors with High on/off Current Ratio and Large Transport Band Gap at Room Temperature. *Nano Lett.* **2010**, *10*, 715–718.

(140) Wi, S.; Kim, H.; Chen, M.; Nam, H.; Guo, L. J.; Meyhofer, E.; Liang, X. Enhancement of Photovoltaic Response in Multilayer MoS_2 Induced by Plasma Doping. *ACS Nano* **2014**, *8*, 5270–5281.

(141) Kwon, H.; Garg, S.; Park, J. H.; Jeong, Y.; Yu, S.; Kim, S. M.; Kung, P.; Im, S. Monolayer MoS_2 Field-Effect Transistors Patterned by Photolithography for Active Matrix Pixels in Organic Light-Emitting Diodes. *npj 2D Mater. Appl.* **2019**, *3*, 9.

(142) Kang, Z.; Cheng, Y.; Zheng, Z.; Cheng, F.; Chen, Z.; Li, L.; Tan, X.; Xiong, L.; Zhai, T.; Gao, Y. MoS2-Based Photodetectors Powered by Asymmetric Contact Structure with Large Work Function Difference. *Nano-Micro Lett.* **2019**, *11*, 1–12.

(143) He, Q.; Zeng, Z.; Yin, Z.; Li, H.; Wu, S.; Huang, X.; Zhang, H. Fabrication of Flexible

MoS_2 Thin-Film Transistor Arrays for Practical Gas-Sensing Applications. *Small* **2012**, *8*, 2994–2999.

(144) Pu, J.; Yomogida, Y.; Liu, K. K.; Li, L. J.; Iwasa, Y.; Takenobu, T. Highly Flexible MoS_2 Thin-Film Transistors with Ion Gel Dielectrics. *Nano Lett.* **2012**, *12*, 4013–4017.

(145) Kim, Y.; Kang, S. K.; Oh, N. C.; Lee, H. D.; Lee, S. M.; Park, J.; Kim, H. Improved Sensitivity in Schottky Contacted Two-Dimensional MoS_2 Gas Sensor. *ACS Appl. Mater. Interfaces* **2019**, *11*, 38902–38909.

(146) Park, J.; Mun, J.; Shin, J. S.; Kang, S. W. Highly Sensitive Two Dimensional MoS_2 Gas Sensor Decorated with Pt Nanoparticles. *R. Soc. Open Sci.* **2018**, *5*, 1–9.

(147) Peng, X.; Han, Y.; Zhang, Q.; Feng, P.; Jia, P.; Cui, H.; Wang, L.; Duan, S. Performance Improvement of MoS_2 Gas Sensor at Room Temperature. *IEEE Trans. Electron Devices* **2021**, *68*, 4644–4650.

(148) Jabbar, H. D.; Fakhri, M. A.; Jalal Abdulrazzaq, M. Gallium Nitride -Based Photodiode: A Review. *Mater. Today Proc.* **2021**, *42*, 2829–2834.

(149) Caldwell, J. D.; Vurgaftman, I.; Tischler, J. G.; Glembocki, O. J.; Owrutsky, J. C.; Reinecke, T. L. Atomic-Scale Photonic Hybrids for Mid-Infrared and Terahertz Nanophotonics. *Nat. Nanotechnol.* **2016**, *11*, 9–15.

(150) Sanders, N.; Bayerl, D.; Shi, G.; Mengle, K. A.; Kioupakis, E. Electronic and Optical Properties of Two-Dimensional GaN from First-Principles. *Nano Lett.* **2017**, *17*, 7345–7349.

(151) Sivula, K.; Le Formal, F.; Grätzel, M. Solar Water Splitting: Progress Using Hematite (α-Fe_2O_3) Photoelectrodes. *ChemSusChem* **2011**, *4*, 432–449.

(152) Hill, A. H.; Jiao, F.; Bruce, P. G.; Harrison, A.; Kockelmann, W.; Ritter, C. Neutron Diffraction Study of Mesoporous and Bulk Hematite, α-Fe_2O_3. *Chem. Mater.* **2008**, *20*, 4891–4899.

(153) Fiori, G.; Bonaccorso, F.; Iannaccone, G.; Palacios, T.; Neumaier, D.; Seabaugh, A.; Banerjee, S. K.; Colombo, L. Electronics Based on Two-Dimensional Materials. *Nat. Nanotechnol.* **2014**, *9*, 768–779.

(154) Briggs, N.; Subramanian, S.; Lin, Z.; Li, X.; Zhang, X.; Zhang, K.; Xiao, K.; Geohegan, D.; Wallace, R.; Chen, L. Q.; Terrones, M.; Ebrahimi, A.; Das, S.; Redwing, J.; Hinkle, C.; Momeni, K.; Van Duin, A.; Crespi, V.; Kar, S.; Robinson, J. A. A Roadmap for Electronic Grade 2D Materials. *2D Mater.* **2019**, *6*, 022001.

(155) Illarionov, Y. Y.; Knobloch, T.; Jech, M.; Lanza, M.; Akinwande, D.; Vexler, M. I.; Mueller, T.; Lemme, M. C.; Fiori, G.; Schwierz, F.; Grasser, T. Insulators for 2D Nanoelectronics: The Gap to Bridge. *Nat. Commun.* **2020**, *11*, 3385.

(156) Zhao, W.; Ghorannevis, Z.; Amara, K. K.; Pang, J. R.; Toh, M.; Zhang, X.; Kloc, C.; Tan, P. H.; Eda, G. Lattice Dynamics in Mono- and Few-Layer Sheets of WS_2 and WSe_2. *Nanoscale* **2013**, *5*, 9677–9683.

(157) Liu, B.; Fathi, M.; Chen, L.; Abbas, A.; Ma, Y.; Zhou, C. Chemical Vapor Deposition Growth of Monolayer WSe2 with Tunable Device Characteristics and Growth Mechanism Study. *ACS Nano* **2015**, *9*, 6119–6127.

(158) Lin, Y. C.; Lin, C. M.; Chen, H. Y.; Vaziri, S.; Bao, X.; Woon, W. Y.; Wang, H.; Liao, S. S. Dielectric Material Technologies for 2-D Semiconductor Transistor Scaling. *IEEE Trans. Electron Devices* **2023**, *70*, 1454–1473.

(159) Laturia, A.; Van de Put, M. L.; Vandenberghe, W. G. Dielectric Properties of Hexagonal Boron Nitride and Transition Metal Dichalcogenides: From Monolayer to Bulk. *npj 2D Mater. Appl.* **2018**, *2*, 6.

(160) Yang, A. J.; Han, K.; Huang, K.; Ye, C.; Wen, W.; Zhu, R.; Zhu, R.; Xu, J.; Yu, T.; Gao, P.; Xiong, Q.; Renshaw Wang, X. Van Der Waals Integration of High-κ Perovskite Oxides and Two-Dimensional Semiconductors. *Nat. Electron.* **2022**, *5*, 233–240.

(161) Ranjan, A.; Raghavan, N.; Holwill, M.; Watanabe, K.; Taniguchi, T.; Novoselov, K. S.; Pey, K. L.; O'Shea, S. J. Dielectric Breakdown in Single-Crystal Hexagonal Boron Nitride. *ACS Appl. Electron. Mater.* **2021**, *3*, 3547–3554.

(162) Hattori, Y.; Taniguchi, T.; Watanabe, K.; Nagashio, K. Anisotropic Dielectric Breakdown Strength of Single Crystal Hexagonal Boron Nitride. *ACS Appl. Mater. Interfaces* **2016**, *8*, 27877–27884.

(163) Hattori, Y.; Taniguchi, T.; Watanabe, K.; Nagashio, K. Layer-by-Layer Dielectric Breakdown of Hexagonal Boron Nitride. *ACS Nano* **2015**, *9*, 916–921.

(164) Jang, S. K.; Youn, J.; Song, Y. J.; Lee, S. Synthesis and Characterization of Hexagonal Boron Nitride as a Gate Dielectric. *Sci. Rep.* **2016**, *6*, 8583–8590.

(165) Liang, S. J.; Cheng, B.; Cui, X.; Miao, F. Van Der Waals Heterostructures for High-Performance Device Applications: Challenges and Opportunities. *Adv. Mater.* **2020**, *32*, 1–27.

(166) Lin, S.; Lu, Y.; Xu, J.; Feng, S.; Li, J. High Performance Graphene/Semiconductor van Der Waals Heterostructure Optoelectronic Devices. *Nano Energy* **2017**, *40*, 122–148.

(167) Liu, Y.; Stradins, P.; Wei, S. H. Van Der Waals Metal-Semiconductor Junction: Weak Fermi Level Pinning Enables Effective Tuning of Schottky Barrier. *Sci. Adv.* **2016**, *2*, 1–7.

(168) Liu, Y.; Guo, J.; Zhu, E.; Liao, L.; Lee, S. J.; Ding, M.; Shakir, I.; Gambin, V.; Huang, Y.; Duan, X. Approaching the Schottky-Mott Limit in van Der Waals Metal-Semiconductor Junctions. *Nature* **2018**, *557*, 696–700.

(169) Kim, S. H.; Han, K. H.; Kim, G. S.; Kim, S. G.; Kim, J.; Yu, H. Y. Schottky Barrier Height Modulation Using Interface Characteristics of MoS_2 Interlayer for Contact Structure. *ACS Appl. Mater. Interfaces* **2019**, *11*, 6230–6237.

(170) Chen, S.; Son, J.; Huang, S.; Watanabe, K.; Taniguchi, T.; Bashir, R.; Van Der Zande, A. M.; King, W. P. Tip-Based Cleaning and Smoothing Improves Performance in Monolayer MoS_2 Devices. *ACS Omega* **2021**, *6*, 4013–4021.

(171) Kim, Y.; Herlinger, P.; Taniguchi, T.; Watanabe, K.; Smet, J. H. Reliable Postprocessing Improvement of van Der Waals Heterostructures. *ACS Nano* **2019**, *13*, 14182–14190.

(172) Jain, A.; Szabó, Á.; Parzefall, M.; Bonvin, E.; Taniguchi, T.; Watanabe, K.; Bharadwaj, P.; Luisier, M.; Novotny, L. One-Dimensional Edge Contacts to a Monolayer Semiconductor. *Nano Lett.* **2019**, *19*, 6914–6923.

(173) Kappera, R.; Voiry, D.; Yalcin, S. E.; Branch, B.; Gupta, G.; Mohite, A. D.; Chhowalla, M. Phase-Engineered Low-Resistance Contacts for Ultrathin MoS_2 Transistors. *Nat. Mater.* **2014**, *13*, 1128–1134.

(174) Zhang, H.; Chiappe, D.; Meersschaut, J.; Conard, T.; Franquet, A.; Nuytten, T.; Mannarino, M.; Radu, I.; Vandervorst, W.; Delabie, A. Nucleation and Growth Mechanisms of Al_2O_3 Atomic Layerdeposition on Synthetic Polycrystalline MoS_2. *J. Chem. Phys.* **2017**, *146*, 052810.

(175) Huang, B.; Zheng, M.; Zhao, Y.; Wu, J.; Thong, J. T. L. Atomic Layer Deposition of High-Quality Al2O3 Thin Films on MoS2 with Water Plasma Treatment. *ACS Appl. Mater. Interfaces* **2019**, *11*, 35438–35443.

(176) McDonnell, S.; Brennan, B.; Azcatl, A.; Lu, N.; Dong, H.; Buie, C.; Kim, J.; Hinkle, C. L.; Kim, M. J.; Wallace, R. M. HfO_2 on MoS_2 by Atomic Layer Deposition: Adsorption Mechanisms and Thickness Scalability. *ACS Nano* **2013**, *7*, 10354–10361.

(177) Borah, A.; Nipane, A.; Choi, M. S.; Hone, J.; Teherani, J. T. Low-Resistance p-Type Ohmic Contacts to Ultrathin WSe_2 by Using a Monolayer Dopant. *ACS Appl. Electron. Mater.* **2021**, *3*, 2941–2947.

(178) Kuila, T.; Bose, S.; Khanra, P.; Mishra, A. K.; Kim, N. H.; Lee, J. H. Recent Advances in Graphene-Based Biosensors. *Biosens. Bioelectron.* **2011**, *26*, 4637–4648.

(179) Yin, Z.; Tang, X. A Review of Energy Bandgap Engineering in III-V Semiconductor Alloys for Mid-Infrared Laser Applications. *Solid. State. Electron.* **2007**, *51*, 6–15.

(180) Hart, J. L.; Hantanasirisakul, K.; Lang, A. C.; Anasori, B.; Pinto, D.; Pivak, Y.; van Omme, J. T.; May, S. J.; Gogotsi, Y.; Taheri, M. L. Control of MXenes' Electronic Properties through Termination and Intercalation. *Nat. Commun.* **2019**, *10*, 522.

(181) Schultz, T.; Frey, N. C.; Hantanasirisakul, K.; Park, S.; May, S. J.; Shenoy, V. B.; Gogotsi, Y.; Koch, N. Surface Termination Dependent Work Function and Electronic Properties of $Ti_3C_2T_x$ MXene. *Chem. Mater.* **2019**, *31*, 6590–6597.

(182) Hajian, S.; Khakbaz, P.; Moshayedi, M.; Maddipatla, D.; Narakathu, B. B.; Turkani, V. S.; Bazuin, B. J.; Pourfath, M.; Atashbar, M. Z. Impact of Different Ratios of Fluorine, Oxygen, and Hydroxyl Surface Terminations on $Ti_3C_2T_x$ MXene as Ammonia Sensor: A First-Principles Study. *2018 IEEE Sensors* **2018**, 1–4.

(183) Gong, C.; Chu, J.; Yin, C.; Yan, C.; Hu, X.; Qian, S.; Hu, Y.; Hu, K.; Huang, J.; Wang, H.; Wang, Y.; Wangyang, P.; Lei, T.; Dai, L.; Wu, C.; Chen, B.; Li, C.; Liao, M.; Zhai, T.; Xiong, J. Self-Confined Growth of Ultrathin 2D Nonlayered Wide-Bandgap Semiconductor CuBr Flakes. *Adv. Mater.* **2019**, *31*, 1–8.

(184) Chin, H.-T.; Wang, D.-C.; Gulo, D. P.; Yao, Y.-C.; Yeh, H.-C.; Muthu, J.; Chen, D.-R.; Kao, T.-C.; Kalbáč, M.; Lin, P.-H.; Cheng, C.-M.; Hofmann, M.; Liang, C.-T.; Liu, H.-L.; Chuang, F.-C.; Hsieh, Y.-P. Tungsten Nitride (W_5N_6): An Ultraresilient 2D Semimetal. *Nano Lett.* **2023**, *24*, 67-73